



Research papers

Detecting and mapping irrigated areas in a Mediterranean environment by using remote sensing soil moisture and a land surface model



Jacopo Dari ^{a,b,d,*}, Pere Quintana-Seguí ^b, María José Escorihuela ^c, Vivien Stefan ^c, Luca Brocca ^d, Renato Morbidelli ^a

^a Dept. of Civil and Environmental Engineering, University of Perugia, via G. Duranti 93, 06125 Perugia, Italy

^b Observatori de l'Ebre (OE), Ramon Llull University – CSIC, 43520 Roquetes, Spain

^c isardSAT, Parc Tecnologic Barcelona Activa, Carrer de Marie Curie, 8, 08042 Barcelona, Spain

^d National Research Council, Research Institute for Geo-Hydrological Protection, via Madonna Alta 126, 06128 Perugia, Italy

ARTICLE INFO

This manuscript was handled by C. Corradini,
Editor-in-Chief

Keywords:
Irrigation
Remote sensing
Soil moisture
Land surface modeling

ABSTRACT

Although irrigation practices affect food production and water resource management, with ever more impacting effects under climate change and population increasing scenarios, detailed knowledge of irrigation is still lacking. In fact, explicit information on the spatial occurrence of irrigation and on the amounts of water used for this purpose is often not available, thus making irrigation the missing variable to comprehensively understand the hydrological cycle dynamics over agricultural areas. Nevertheless, remote sensing techniques can be used to delimit the irrigation extent.

In this study, the capability of five remotely sensed soil moisture products to detect the irrigation signal over an area intensely equipped for irrigation in the North East of Spain is investigated; moreover, a method to map the actually irrigated areas based on the K-means clustering algorithm is proposed. The remote sensing soil moisture data sets used in this study are SMOS (Soil Moisture and Ocean Salinity) at 1 km, SMAP (Soil Moisture Active Passive) at 1 km and 9 km, Sentinel-1 at 1 km, and ASCAT (Advanced SCATTERometer) at 12.5 km. The 1 km resolution versions of SMOS and SMAP are obtained by downscaling coarser SMOS and SMAP data through the DISPATCH (DISSaggregation based on Physical And Theoretical scale CHange) algorithm. The analyses are supported by an additional data set of soil moisture at 1 km resolution simulated by the SURFEX-ISBA (SURFace EXternalisée – Interaction Sol Biosphère Atmosphère) land surface model.

Among all the considered data sets, the L-band passive microwave downscaled products show the best performances in detecting the irrigation signal over the pilot area, especially SMAP at 1 km. The proposed maps of irrigated areas derived by exploiting soil moisture from SMAP at 1 km data set agree well (up to 78%) with the ground truth derived irrigated areas. Furthermore, the method is able to well distinguish the actually irrigated areas from rainfed agricultural areas, thus representing a useful tool to obtain reliable spatial information about the areas where irrigation actually occurs.

1. Introduction

Human-induced changes on the hydrological cycle nowadays rival the geophysical processes, with short-term impacts that can be steeper than the effects of climate changes. Irrigation is the anthropogenic activity that introduces the largest imbalances in the natural hydrological cycle at different spatial scales (Wada et al., 2014; Alter et al., 2015). In the past decades, the irrigation practices allowed to double the agricultural production despite an increase of cropland by only 12%

(Rosegrant et al., 2002; Gleick, 2003). It is estimated that over 70% of global freshwater withdrawals are destined to irrigation practices (Foley et al., 2011), with the major rates of water consumption attributable to Northern America, Europe, Northern India and Eastern China (Zhou et al., 2016). The ever growing global population and consequent increases of food requirements, combined with rising global mean temperatures, are expected to further stress the freshwater availability for irrigation purposes, especially over areas already facing water scarcity (Vörösmarty et al., 2000; Rockström et al., 2012; Kummu et al., 2016). It

* Corresponding author at: Dept. of Civil and Environmental Engineering, University of Perugia, via G. Duranti 93, 06125 Perugia, Italy.
E-mail address: jacopo.dari@unifi.it (J. Dari).

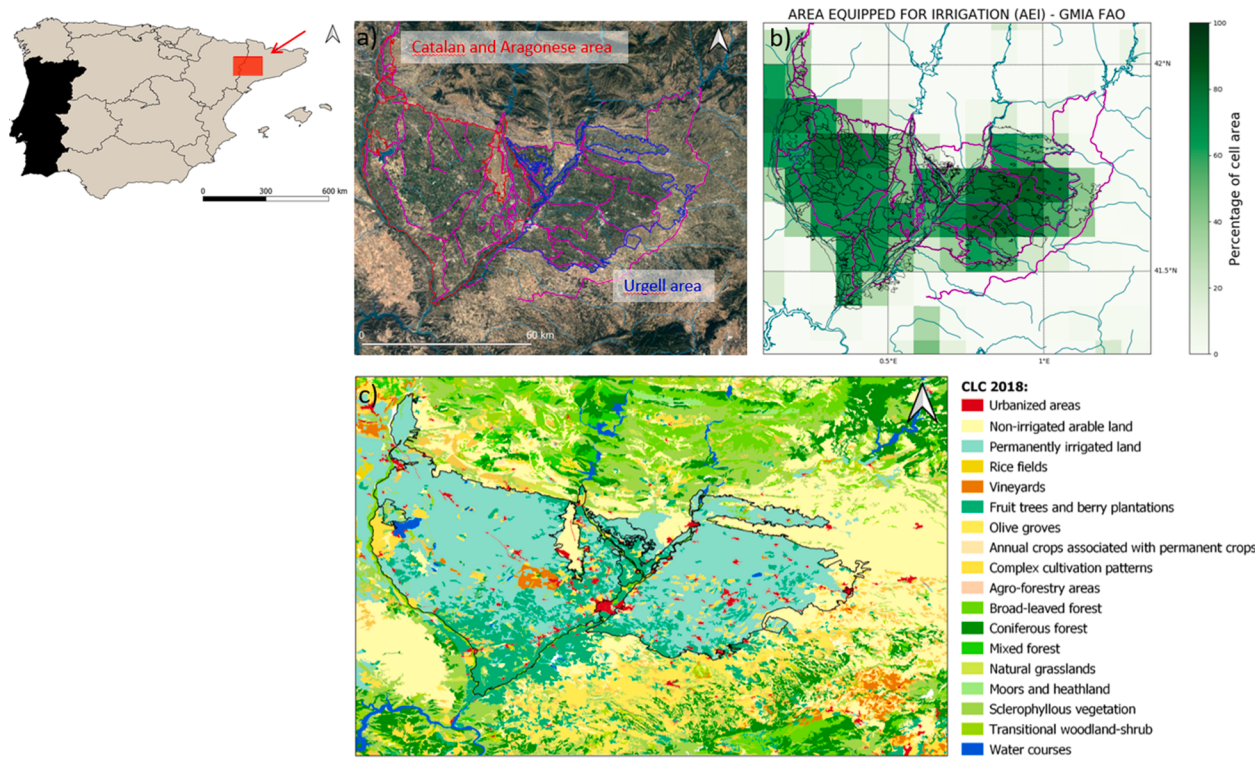


Fig. 1. Overview of the study area: a) location with respect to Spain (in the top left map Portugal has been overshadowed), b) percentage of area equipped for irrigation according to GMIA – FAO, and c) land cover map according to CLC for the year 2018. In a) and b) the irrigation canals network is represented in magenta. (For interpretation of the references to colour in this figure legend, the reader is referred to the web version of this article.)

appears clear that, under this scenario, a rational management of irrigation practices is required. Methods to retrieve information about irrigation water volumes (Romaguera et al., 2014; Brocca et al., 2018; Jalilvand et al., 2019; Dari et al., 2020; Filippucci et al., 2020) and the detailed knowledge of the irrigation extent (Kumar et al., 2015; Ambika and Mishra, 2016; Gao et al., 2018; Zaussinger et al., 2019) are challenging targets for the development of sustainable agricultural practices and for the water resource management in the upcoming decades.

The rise of remote sensing has led to new perspectives in monitoring irrigated lands; this technology has proven to be a promising tool for mapping the exact locations and spatial extensions of irrigated areas, thus enhancing approximate statistical information within arbitrary political edges (Ozdogan et al., 2010). Several studies have investigated the detectability of irrigation signals by using optical data only (Ozdogan and Gutman, 2008; Peña-Arancibia et al., 2014; Ambika and Mishra, 2016), optical data supported by land surface modeling (Romaguera et al., 2014; Hain et al., 2015), microwave data only (Lawston et al., 2017; Gao et al., 2018) and microwave data supported by land surface modeling (Kumar et al., 2015; Escorihuela and Quintana-Seguí, 2016). The first study exploiting microwave sensors to detect irrigated areas was carried out by Kumar et al. (2015), who investigated the capability of several remotely sensed soil moisture products to detect irrigation over the CONUS (CONtiguous United States) area. The data sets used were ASCAT (Advanced SCATterometer), AMSR-E (Advanced Micro-wave Scanning Radiometer – Earth Observing System), ESA CCI SM (European Space Agency Climate Change Initiative Soil Moisture), SMOS (Soil Moisture and Ocean Salinity) and Windsat. The detection of irrigated areas was supported by comparisons with modeled soil moisture obtained by the Noah land surface model, which does not take into account of irrigation. Hence, positive biases between satellite and modeled soil moisture data were interpreted as a signal of irrigation. Only ASCAT showed some potential in detecting irrigation over wide irrigated areas in the plains of Nebraska. Over the same area, Zaussinger et al. (2019) found scarce correlation between ASCAT retrieved and

MERRA-2 (Modern-Era Retrospective analysis for Research and Applications 2) reanalysis soil moisture in absence of precipitation; however, a similar pattern was also found over rainfed agricultural areas. Escorihuela and Quintana-Seguí (2016) compared four soil moisture products (ASCAT, AMSR-E, SMOS and a version of SMOS at 1 km obtained by downscaling the original product through the DISaggregation based on Physical And Theoretical scale CHange, DISPATCH, algorithm) with soil moisture simulated by the SURFEX-ISBA (SURface EXternalisée – Interaction Sol Biosphère Atmosphère) land surface model over the Northeast of the Iberian Peninsula. The results pointed out the potential of the high-resolution version of SMOS to detect the irrigation signal in terms of low correlation with modeled soil moisture over an intensely irrigated area, the Urgell, in the Catalonia autonomous community; over areas with a similar flat topography, but not irrigated, higher correlations were obtained. Lawston et al. (2017) showed the capability of the enhanced 9 km version of SMAP (Soil Moisture Active Passive) to detect the irrigation signal over three semiarid regions in the Western United States. Very recently, Gao et al. (2018) exploited Sentinel-1 SAR (Synthetic Aperture Radar) time series to map irrigated fields over an agricultural site in the Urgell, Catalonia (Spain). However, studies exploiting remote sensing soil moisture to map irrigation over areas where high-resolution products are needed are still lacking; in fact, irrigation is practiced worldwide at different spatial scales, depending on several factors (e.g., the topography or climate). This work is aimed at showing the capability of high-resolution products in detecting irrigation occurring at a spatial scale compatible with the Mediterranean environment.

As a first objective of this study, the capability of five remotely sensed soil moisture products to detect irrigation during the biennium 2016–2017 over an intensely irrigated area located in Spain is evaluated. Three of the considered data sets are high-resolution (1 km) products: SMOS at 1 km, SMAP at 1 km and Sentinel-1; the first two products are downscaled versions of coarser resolution SMOS and SMAP data, obtained through the DISPATCH algorithm (Merlin et al., 2013). The other two products used in this study have a coarser resolution, and

are the enhanced version of SMAP (9 km sampling) and ASCAT (12.5 km sampling). The choice of the data sets is related to the extent of the pilot area and it is mainly oriented on high-resolution (1 km) products; however, the two coarser resolution data sets have been included in order to perform a comprehensive analysis involving medium to high resolution products obtained through different operational bands. An additional data set of modeled soil moisture at 1 km obtained by forcing the SURFEX-ISBA land surface model with atmospheric data from ERA-5 reanalysis resampled at the same resolution is used as a support for the analyses. As a secondary objective, a method to map the actually irrigated areas based on the K-means clustering algorithm and exploiting the best performing products over the study area is proposed.

2. Study area

The study area is located in the North Eastern part of Spain, within the Ebro river basin and has an extension of about 125 km × 80 km; a part of it falls in Catalonia, while the other part is inside Aragon. This tile encloses an irrigated land surrounding the city of Lleida. An overview of the study area is given in Fig. 1, which shows where the area is located, the map of the area equipped for irrigation and the land cover map. The area equipped for irrigation is derived from the Global Map of Irrigated Areas (GMIA) – version 5.0 produced by the Food and Agriculture Organization of the United Nations, FAO (Siebert et al., 2013). The data is expressed as the percentage of each cell area that is equipped for irrigation and has a spatial resolution of 5 arc-minutes (about 10 km at the Equator). The land cover map is derived from the Corine Land Cover (CLC) provided by the Copernicus Land Monitoring Service; the map has a 100 m resolution and it is referred to the year 2018. According to the structure of the irrigation canals network, it is possible to distinguish two different irrigated portions within the pilot area: the first one (henceforth Urgell area) mainly supplied by the Urgell and the Algerri-Balaguer canals, in the East side and the second one (henceforth Catalan and Aragonese area) mainly supplied by the Catalan and Aragonese canal, in the West side. Within the Urgell area, different irrigation systems coexist; in the old irrigation district, the most used system is inundation, while in Algerri Balaguer, drip irrigation is typically used for fruit trees and sprinkler irrigation is used for crops. The irrigation systems in the area supplied by the Catalan and Aragonese canal are flood irrigation (18% of the area), sprinkler irrigation (54%) and drip irrigation (28%). These differences in the adopted irrigation methods contribute in making the irrigated fields more scattered. Within this area, several pivot infrastructures can be observed. The timing of the irrigation practices depends on several factors (e.g. the crop type), but they are mainly concentrated during the summer period, from May to September. The frequency depends on the irrigation technique; for example, within the Urgell, in the old system inundation irrigation occurs typically every two weeks, while in modern irrigated areas irrigation can occur every day. In both areas, summer cereals and forage are present. Fruit trees are spread in the south of both irrigated lands, in the east of Urgell and along the river channel that divides the two areas. In the Catalan and Aragonese domain, there is an area destined to vineyard.

Towards the East of Urgell, there is a wide area of rainfed cropland, which is connected to the South to olive groves through a mixed zone of sparse shrubs; this entire portion is generally dry during summer, thus creating an extended dryland that is in contrast with the irrigated areas, which appear lush. Especially in the dry season, the two strongly different wetness conditions coexisting in the area of interest contribute in making it an optimal site to test the capability of remote sensing data to spot where irrigation practices occur.

3. Materials and methods

3.1. Remote sensing data

In this study, five soil moisture products have been considered: SMOS at 1 km, SMAP at 1 km and 9 km, Sentinel-1 at 1 km, and ASCAT at 12.5 km. The first two products are obtained by downscaling coarser SMOS and SMAP data through the DISPATCH algorithm.

3.1.1. SMOS

The SMOS mission was launched by the European Space Agency (ESA) in November 2009 (Kerr et al., 2001, 2010) to collect global measurements of soil moisture over the continents and of salinity over the oceans; it is the second ESA's Earth Explorer Opportunity mission, which is jointed with the *Centre National d'Etudes Spatiales* (CNES) and the *Centro para el Desarrollo Tecnológico Industrial* (CDTI). The revisit period of SMOS is 3 days at the Equator, which is crossed at 06:00 and 18:00 Local Solar Time (LST) during the ascending and descending orbits, respectively. The SMOS satellite carries an Y-shaped passive 2D interferometric radiometer working at L-band frequency (1.4 GHz) and is capable to collect multiangular observations of the brightness temperature, thus retrieving surface soil moisture and other parameters. The original SMOS soil moisture data has a spatial resolution ranging between 35 and 50 km and is obtained through the Level-2 (L2) retrieval algorithm, which exploits additional static (soil texture, topography index, land use) and dynamic (rain, temperature, frost and thaw cycle) data sets (Kerr et al., 2012). In this study, a high-resolution (1 km) DISPATCH downscaled version (Merlin et al., 2008) is used. The DISPATCH method allows to downscale SMOS surface soil moisture from low resolution (about 40 km) to high resolution (1 km) by using the Normalized Difference Vegetation Index (NDVI) and the Land Surface Temperature data, both at 1 km resolution, detected by MODIS (Moderate resolution Imaging Spectroradiometer) sensor aboard Terra (EOS AM) and Aqua (EOS PM) satellites. The disaggregation of coarser soil moisture data is performed by separating the evaporation from the surface soil layer (0–5 cm) and the transpiration from the root zone due to the vegetation. Hence, the Soil Evaporative Efficiency (SEE), defined as the ratio of actual to potential evaporation, can be estimated over the bare soil. The spatial link between the optical-derived SEE and the near-surface soil moisture allows to distribute the high-resolution soil moisture around the mean value of the low-resolution product (Merlin et al., 2012), providing outputs with the same temporal resolution of the coarser resolution input data. The DISPATCH method does not require in situ observations to disaggregate coarse resolution data, but its applicability is limited to cloudless conditions (Peng et al., 2017). However, when there are clouds, the algorithm attributes the low resolution soil moisture value to the high resolution pixel. Merlin et al. (2013) compared SMOS soil moisture at 40 km and two DISPATCH disaggregated versions at 3 km and 100 m with in situ measurements aggregated at the same spatial scales over pilot sites in Catalonia and observed enhancements of the spatio-temporal correlation when considering the downscaled products. In fact, a value of correlation equal to 0.59 was found for the 40 km resolution product, while correlation values were 0.67 for the 3 km version and 0.73 and 0.86 for two different configurations of the 100 m resolution product. A similar study was carried out by Malbéteau et al. (2015), which evaluated the performances of coarse and DISPATCH downscaled (1 km) versions of SMOS and AMSR-E soil moisture products against in situ observations over the South East of Australia. The study highlighted enhancements in the correlation with ground measurements over a semi-arid region obtained during summer for the disaggregated products with respect to their coarser resolution versions. Correlation values increased from 0.37 to 0.63 and from 0.47 to 0.73 in afternoon overpasses for SMOS and AMSR-E, respectively, and from 0.63 to 0.78 and from 0.42 to 0.71 in morning overpasses for SMOS and AMSR-E, respectively. Molero et al. (2016) evaluated the performances of DISPATCH downscaled SMOS at

1 km under different climatic conditions, obtaining higher correlations with ground observations over semi-arid areas (where the spatio-temporal variability of soil moisture is mainly determined by precipitation and irrigation) with respect to sub-humid regions.

3.1.2. SMAP

The SMAP mission was launched by the National Aeronautics and Space Administration (NASA) at the end of January 2015, with the aim of collecting soil moisture data and to detect the freeze/thaw state at global scale (Entekhabi et al., 2010). SMAP has a revisit period of 2–3 days at the Equator, which is overpassed at 06:00 LST during the descending orbit and at 18:00 LST during the ascending orbit. Originally, SMAP was supposed to enhance the resolution of radiometer-only retrievals by combining the benefits of active and passive remote sensing through an L-band radar (1.26 GHz) and an L-band radiometer (1.4 GHz), thus providing surface soil moisture measurements at three different resolutions: 3 km, 9 km and 36 km. Unfortunately, the radar stopped working only a few months after the launch, so only the 36 km and the enhanced 9 km products have been delivered during the post-radar period. However, a 3 km version obtained by merging with data retrieved by Sentinel-1A/Sentinel-1B has been recently released (Das et al., 2019). The 9 km sampling product, whose complete name is SMAP Level 2 Enhanced Passive Soil Moisture Product (L2_SM_P_E), is obtained after the interpolation of the antenna temperature data in the SMAP original Brightness Temperature Product through the Backus-Gilbert technique (Poe, 1990; Stogryn, 1978) and several calibration and correction processes (Chan et al., 2018).

Both SMOS and SMAP radiometers operate within the protected Earth Exploration Satellite Service passive frequency allocation of 1400–1427 MHz. However, unauthorized in-band transmitters and out-of-band emissions from transmitters operating at frequencies adjacent to this allocated spectrum cause interference to microwave radiometry in this band. Thanks to SMOS it was realised that Radio-Frequency Interference (RFI) was affecting measurements in this protected band and the SMAP radiometer included a special flight hardware to enable the detection and filtering of RFI.

In this study, we use the 9 km sampling version (O'Neill et al., 2016) and a 1 km resolution version derived through the DISPATCH downscaling algorithm described in the previous section.

3.1.3. Sentinel-1

The Sentinel-1 constellation is the first of the six missions developed by ESA for Copernicus, the European Earth observation program, and consists of two identical satellites, Sentinel-1A and Sentinel-1B launched in April 2014 and April 2016, respectively. The Sentinel-1 satellites carry a single SAR operating at C-band frequency (C-SAR, 5.4 GHz), which is capable to collect measurements in four different ways; the one of interest for soil moisture observations is the Interferometric Wide swath (IW) mode. The data detected through this technique are the basis of the production of the Sentinel-1 Surface Soil Moisture (SSM), delivered by the Copernicus Global Land Service and used in this work. Since 2016, when both the satellites of the Sentinel-1 constellation are operational, the coverage over Europe is guaranteed with a revisit time ranging between 1.5 and 4 days, but it can go down up to 6 days over the rest of the Earth. The Sentinel-1 SSM is retrieved by adapting to high resolution SAR data the change detection algorithm (Wagner et al., 1999; Hornáček et al., 2012) originally developed by the Vienna University of Technology (Bauer-Marschallinger et al., 2018). The soil moisture product is delivered with three masks, one for water areas, one for pixels with low sensitivity and one for excessive terrain slope.

3.1.4. ASCAT

The ASCAT remote sensing instrument on board of the EUMETSAT Meteorological Operational satellites (METOP series) is a real aperture active radar operating at C-band frequency (5.3 GHz) and using vertically polarized antennas. The first satellite of METOP series, METOP-A,

was launched in October 2006; METOP-B was launched later, in September 2012, in order to ensure the continuity of observations after the end of METOP-A operational life. The last METOP satellite, METOP-C, was launched in November 2018. ASCAT global coverage is obtained every 1–3 days and the Equator is overpassed at 21:30 during the ascending pass and at 09:30 during the descending pass. Originally, ASCAT was designed to monitor wind speed and direction over the oceans and was not supposed to collect soil moisture observation, but studies focused on the antecedent version of the instrument, ESCAT, proved the suitability of ASCAT in monitoring soil moisture (Pulliainen et al., 1998; Wen and Su, 2003; Wagner et al., 2007). The ASCAT soil moisture product is obtained through the change detection algorithm (Wagner et al., 1999, 2013; Bartalis et al., 2007; Naeimi et al., 2009) developed by the Vienna University of Technology and is furnished as degree of saturation, ranging between 0 and 1. ASCAT soil moisture has a spatial resolution of 25 km and is provided resampled on a 12.5 km grid. In this study, the H115 soil moisture product distributed by EUMETSAT H SAF, and available from 2007 to 2018, is used.

3.2. SURFEX modeling platform

The modeled soil moisture data set used in this study is obtained from the SURFEX modeling platform (Masson et al., 2013) developed by Météo-France. SURFEX allows to calculate the surface fluxes and it consists of independent physical schemes that allow describing four different kind of surfaces: natural surfaces, urbanized areas, inland water and oceans. In the study presented here, only the ISBA scheme, for natural surfaces, has been used. ISBA (Noilhan and Planton, 1989; Mahfouf and Noilhan, 1996; Noilhan and Mahfouf, 1996) contains several algorithms to compute the exchanges of energy and water between the surface (soil-vegetation-snow continuum) and the atmosphere. Several versions of the ISBA scheme have been developed in time (Boone et al., 1999; Boone, 2000; Habets et al., 2003). In this study, the ISBA-DIF version is used, where the soil is divided in N layers, with N equal to 14 by default and the root zone has a variable extension depending on vegetation. Simulations have been carried out at 1 km resolution by using the latest version of the model, SURFEX v8.1, obtained from the *Centre National de Recherches Météorologiques*. In general, 1D hydrological assumptions adopted in land surface models (as the absence of lateral flows in SURFEX-ISBA) are expected to become less valid with the increase of the resolution at which simulations are performed; however, in the pilot area lateral flows are supposed to be negligible and thus the missing modeling of such processes is expected to be not relevant. In fact, the study area is dry and rather flat, especially over the irrigated land, thus lateral flows are of several orders of magnitude lower than vertical flows (e.g., evapotranspiration, infiltration, drainage). In the performed simulation, a prescribed vegetation scheme based on the climatology of the Leaf Area Index (LAI) has been adopted; hence, the vegetation is the same every year. This simplified approach has been preferred to a more accurate interactive vegetation scheme available in SURFEX-ISBA, as in this study the modeling part has been involved with the aim of showing the soil moisture distribution in absence of irrigation and the adopted approach is able to represent the first order effects of a lack of irrigation without adding complexity to the modeling. It is noteworthy that a new irrigation scheme has been implemented in the next version of SURFEX to be released (Druel et al., 2019); in this configuration, ISBA is able to simulate sprinkler, drip, and flood irrigation over irrigated areas experiencing a soil moisture deficit.

The atmospheric data to force the model are taken from the ERA-5 reanalysis (Hersbach et al., 2020) released by the European Centre for Medium-Range Weather Forecast (ECMWF). The ERA-5 data, provided at a spatial resolution of $0.25^\circ \times 0.25^\circ$, has been downloaded from the Copernicus Climate Data Store; in order to run SURFEX-ISBA, hourly data of 2 m air temperature and relative humidity, precipitation, wind speed, and downward visible and infrared radiation are needed. It is noteworthy that, although the input data is at an hourly time step, the

model's internal step is of higher resolution (15 min). Before the simulation, the input atmospheric variables have been resampled to the finer grid of the model (1 km); furthermore, a lapse rate correction to temperature and relative humidity has been performed to overcome the vertical mismatch between the coarse resolution relief of ERA-5 and the high-resolution relief (GTOPO30) adopted in SURFEX. Recently, Albergel et al. (2018) showed the benefits of forcing ISBA simulations with ERA-5 atmospheric data in terms of the good representation of the surface variables linked to the terrestrial hydrological cycle, e.g., soil moisture. The modeled surface soil moisture used in this study is referred to the first 4 cm of soil and is obtained by the weighted average between the first two layers of the soil parametrization, whose thicknesses are up to 1 cm and up to 4 cm, respectively.

3.3. Temporal stability

The temporal stability theory is a well-established method originally introduced by Vachaud et al. (1985) to identify optimal soil moisture measurement points within a certain area. This technique has been widely applied in studies aimed to optimize the soil moisture monitoring (see, e.g., Brocca et al., 2010; Gao et al., 2015; Dari et al., 2019) or the raingauge network design (Morbidelli et al., 2019). In this study, the key variables of the method are used to calculate indices expressing the dynamics of soil moisture both in space and time.

Let θ_{xt} be the soil moisture, observed or modeled, at the pixel x of the grid and at the day t . Assuming that $\bar{\theta}_t$ is the spatial mean of soil moisture referred to the whole area and to each day, the relative differences, δ_{xt} , for each pixel and for each day, are given by:

$$\delta_{xt} = \frac{\theta_{xt} - \bar{\theta}_t}{\bar{\theta}_t} \quad (1)$$

for each pixel x , the temporal mean, $\bar{\delta}_x$, and the standard deviation, $\sigma(\delta_x)$, can be calculated by:

$$\bar{\delta}_x = \left(\frac{1}{T} \right) \sum_{t=1}^T \delta_{xt} \quad (2)$$

$$\sigma(\delta_x) = \sqrt{\left(\frac{1}{T-1} \right) \sum_{t=1}^T (\delta_{xt} - \bar{\delta}_x)^2} \quad (3)$$

where T is the total number of considered days.

The relative difference is an index giving information about the spatial variability of soil moisture. The perspective proposed by Mittelbach and Seneviratne (2012) allows to investigate also the temporal dynamics of soil moisture by exploiting the anomalies. The temporal anomalies, A_{xt} , quantify how much the soil moisture at pixel x differs from its temporal mean and can be calculated as follows:

$$A_{xt} = \frac{\theta_{xt} - \bar{\theta}_x}{\bar{\theta}_x} \quad (4)$$

where $\bar{\theta}_x$ is the temporal mean referred to pixel x . \bar{A}_x and \bar{A}_t indicate the temporal and spatial mean of temporal anomalies, respectively.

3.4. K-means clustering

K-means is one of the most widespread clustering algorithms. It allows to group n data points into k clusters on the basis of predefined characteristics. Each cluster is identified by a centroid determined through an iterative process starting from a first attempt randomly chosen among the input data; then, the algorithm associates each data point to the nearest centroid, thus grouping elements with the same features. The association of each element to its cluster is performed by minimizing the Euclidean distance, d , between the input vector and the centroids vector:

$$d = \sum_{i=1}^k \sum_{j=1}^n \|x_j - C_i\| \quad (5)$$

where x_j is the j -th element of the input vector, with $j = 1, \dots, n$ and C_i is the i -th centroid, with $i = 1, \dots, k$. More details on the algorithm can be found in MacQueen (1967).

In this study, the K-means algorithm is employed to classify, on the basis of satellite and modeled soil moisture, three kinds of surfaces within the study area: the area actually irrigated, the dryland, and forest or natural areas. Four sets of features are used to group the data into the three clusters; the first set is composed by the standard deviation of the relative differences and the mean temporal anomaly calculated for the satellite soil moisture, the second set is composed by the mean relative difference and the mean temporal anomaly derived from the satellite soil moisture, in the third and fourth sets respectively, the correlation between satellite and modeled soil moisture is added to the previous two parameters. For each year, all the considered features are referred to the period ranging from May to September, when irrigation mainly occurs.

3.5. Ground truth data

The ground truth data set used in this study is the map of crops in Catalonia for the years 2016 and 2017 distributed by the *Department d'Agricultura, Ramaderia, Pesca i Alimentació*. It is an open access map produced in the same domain of the Geographic Information System for Agricultural Parcels (SIGPAC) available at <http://agricultura.gencat.cat/ca/serveis/cartografia-sig/aplicacions-temàtiques-geoinformacio/sigpac/mapa-cultius/>. The map is produced by integrating the agricultural parcels data produced by SIGPAC with the *Declaració Unica Agrària* (DUN) document, which consists in a yearly mandatory declaration about the agricultural exploitation that each owner of an agricultural productive area must provide. In order to optimize the product, some corrections are performed before its delivering. The non-cultivated areas (forest, urban areas, pastures and unproductive areas) are masked out, the parcels smaller than 50 m² and those with incomplete DUN documents are deleted and some geometry points are simplified; however, these corrections reduce the originally declared area by less than 1%. For each plot, the resulting yearly crops maps contain information about the geographic and administrative localization, the type of cultivated product, the irrigation coefficient and the extension.

In this study, the SIGPAC crops maps have been used as the ground truth data set to validate the K-means retrieved classification maps. Two kind of validations have been performed; the first one exploits the irrigation coefficient information, while in the second one the attribute regarding the kind of crop is used. Unfortunately, the ground truth data set is available for Catalonia autonomous community only, so the validations have been performed over an area equal to the 71% of the total. In addition, an analysis of the sensitivity of the classification accuracy to the aggregation threshold of the original ground truth data has been performed and it is provided in the Appendix A.

3.6. Data preparation

3.6.1. Remote sensing data

All the remote sensing soil moisture data sets used have been resampled to the 1 km grid used for the SURFEX-ISBA simulations. This process allowed to obtain spatially coherent data to carry out the analyses described in this study.

3.6.2. Ground truth data

The ground truth data set has been pre-processed. For the first of the two validations, a map of irrigated crops, dryland and forest or natural areas has been produced on the basis of SIGPAC data. The original data has a plot scale resolution, so as a first step the information has been projected on a 100 m resolution regular grid over the study area, thus

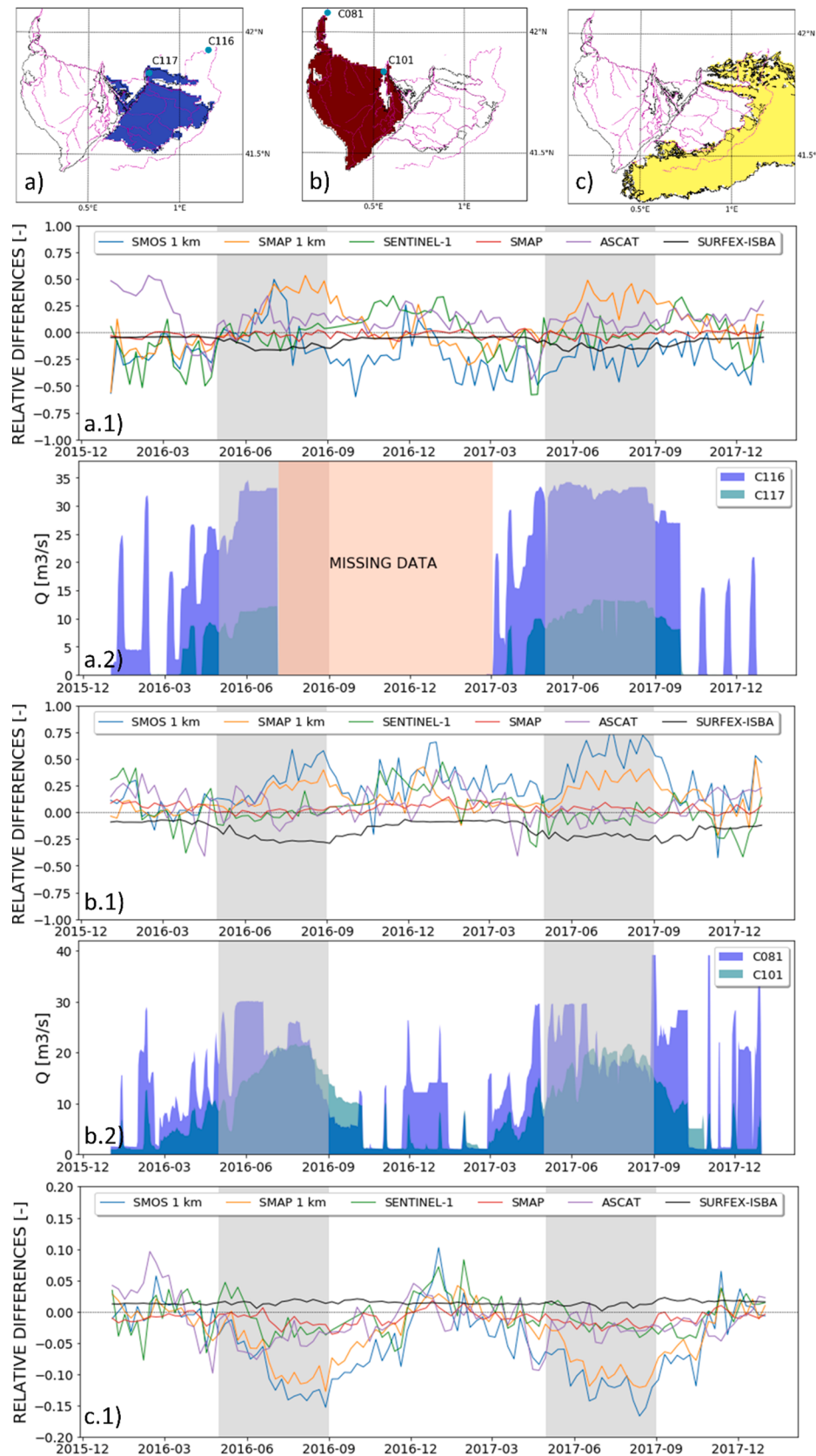


Fig. 2. The panels a.1), b.1) and c.1) show the time series of the weekly spatial relative differences averaged inside the corresponding areas: a) Urgell area, b) Catalan and Aragonese area, and c) the dryland. The panels a.2) and b.2) show the daily flow in the canals feeding the Urgell and the Catalan and Aragonese areas, respectively. Note the different y-axis range for the panel c.1).

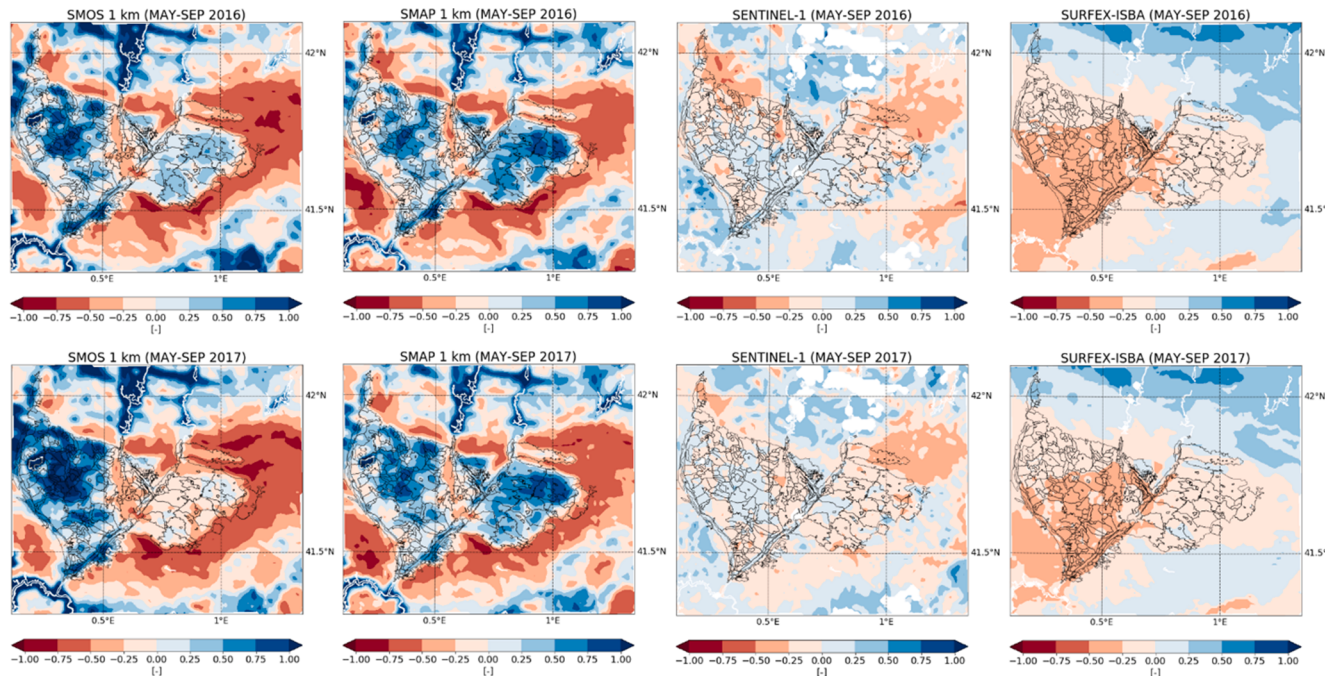


Fig. 3. Maps of the spatial relative differences averaged during the periods May–September 2016 (upper panel) and May–September 2017 (lower panel).

producing a map with irrigated pixels and dryland pixels where the information about the irrigation coefficient in ground truth data set provides irrigation and non-irrigation, respectively. Elsewhere, where the ground truth data set has no data, the pixel has been classified as forest or natural area. Actually, this procedure is not expected to introduce large errors, because the crops maps are produced starting by land use maps provided by SIGPAC and masking exactly this kind of surfaces with the addition of urban areas, that we mask together with water bodies before the validation. The resulting maps at 100 m resolution have then been resampled to the 1 km grid used to run SURFEX-ISBA simulations by assigning to each pixel of 1 km × 1 km the predominant class among those of the 100 m × 100 m pixels contained in it. Only in the case of distinguishing between dryland and forest or natural area, an additional condition has been added: a 1 km × 1 km pixel, in order to be classified as forest or natural, must contain 100 m × 100 m pixels with the forest or natural class as dominant one and the pixels with this attribute must be at least the double of those non-irrigated. This condition is necessary to classify in a homogeneous class complex landscapes like the one in the south of the Urgell area, where it is difficult to clearly distinguish between the forest, the shrubs areas and olive trees that are highly mixed.

The SIGPAC classification between irrigated/non-irrigated refers to the capability of the field to be reached by the irrigation network, but does not necessarily imply that the field is actually irrigated (it may happen for instance that the field irrigation infrastructure is not installed). For this reason, a second validation has been carried out by exploiting the information about the type of cultivation. Among the irrigated plots, those with crops that for sure are irrigated in the period May–September have been selected: they are summer cereals, forage and fruit trees. Pixels with this information have been classified as irrigated, while pixels with information linked to other crops (e.g., cereals or olive groves) have been classified as dryland; the remaining pixels have been considered as forest or natural areas. The final product used for the validation is at 1 km resolution and it is obtained with the same procedure previously described.

4. Results

Henceforth, we call the downsampled products “SMOS at 1 km” and

“SMAP at 1 km”, while the others “Sentinel-1”, “SMAP” and “ASCAT”. Although the study covers the whole period 2016–2017, many results are focused on a time span of four months, from May 1st to September 1st of the two considered years, when the irrigation practices reach the maximum intensities. In subsection 4.1 the analysis performed on the basis of the temporal stability derived indices is presented, while subsection 4.2 presents the results of the classification performed through the K-means clustering.

4.1. Indices derived from the temporal stability theory

4.1.1. Spatial relative differences

The most immediate temporal stability derived index to test the capability of a soil moisture product to detect the irrigated areas is the spatial relative difference. It quantifies how much the soil moisture in a site during a certain day differs from the spatial mean for the same day; hence, a soil moisture product able to detect irrigation should provide higher values of relative differences over the irrigated areas, which are human induced to be wet during the dry season. The peculiarity of the study area, where the irrigation districts are surrounded by dryland during summer, is expected to emphasize this behaviour. In Fig. 2, the panels a.1), b.1), and c.1) show the time series of the areal mean relative differences calculated for the Urgell area, for the Catalan and Aragonese area and for the dryland, respectively; for each product, the same colour has been kept for time series referred to the three areas. The panels a.2) and b.2) show the time series of the water flowing through the irrigation canals network and feeding the Urgell and the Catalan and Aragonese area, respectively. The records of the flow data supplying the Urgell are taken from the stations “C116-Cabecera Urgell” and “C117-Auxiliar de Cabecera Urgell”, while for the Catalan and Aragonese area the stations of interest are “C081-El Ciego” and “C101-Coll de Foix”; the data about the irrigation systems flow is delivered by the Automatic Hydrologic Information System of the Ebro river basin (SAIH Ebro) at the website: <http://www.saihebro.com/saihebro/index.php?url=/datos/canales>. During the period going from July 2016 to the end of February 2017, the data about irrigation water supplying the Urgell are missing.

The capability of a satellite product in containing information about irrigation in terms of the relative difference is evaluated by looking at which data set shows higher values of this index inside the irrigated

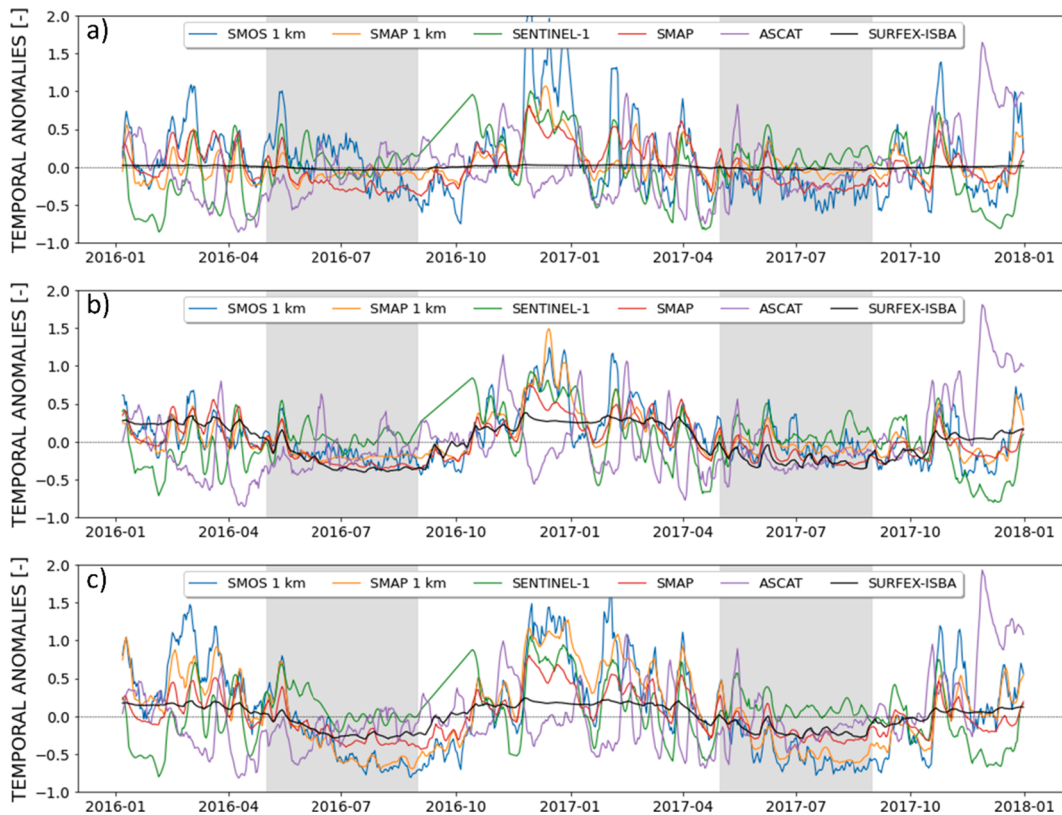


Fig. 4. Time series of the 7-days moving average of the mean temporal anomalies for each corresponding area: a) Urgell area, b) Catalan and Aragonese area, and c) dryland.

areas concurrently with lower values in the dryland, during the periods May-September 2016 and 2017. In the Urgell, SMAP at 1 km results the best performing high-resolution product, with a mean relative difference equal to 0.274 during May-September 2016 and equal to 0.266 during May-September 2017, while in the dryland the corresponding values for the same periods are equal to -0.078 and to -0.088 . SMOS at 1 km performs well only for a part of the focus period in 2016, while Sentinel-1 does not show clear irrigation signals. Among the coarser resolution products, in the Urgell, ASCAT performs better than SMAP, showing values of the mean relative difference equal to 0.121 and to 0.111 for May-September 2016 and 2017, respectively; the corresponding values for the same periods but referred to the dryland are equal to -0.045 and to -0.023 .

Over the Catalan and Aragonese area, SMOS at 1 km is the best performing high-resolution product, with values of the mean relative difference equal to 0.286 and to 0.481 for the periods May-September 2016 and 2017, respectively; the values of the same indices and referred to the same periods but calculated over the dryland result equal to -0.100 and -0.112 . SMAP at 1 km also shows good performances, comparable to those from SMOS at 1 km, while Sentinel-1 still does not show a clearly interpretable irrigation signal. The coarser resolution products do not show good performances in the Catalan and Aragonese domain.

It is noteworthy that, during summer 2016 and 2017, the time series of the relative differences derived from SURFEX-ISBA modeled soil moisture, which does not take into account of irrigation, show slightly lower values than the areal mean relative differences for both the irrigation districts, while outside the irrigated areas the trend is temporally constant. This behaviour can be likely attributed to the vegetation and soil map implemented in the model, which regulate the spatial distribution of soil moisture. As explained in subsection 3.2, in the adopted version of ISBA the LAI cycle and thus the cycle of the vegetation is the same every year, because its evolution is determined by the climatology.

The maps of the spatial relative differences averaged during the periods May-September 2016 and 2017 are shown in Fig. 3. Because of the extension of the pilot area, only the maps referred to the high-resolution products are shown; the maps obtained from the coarser resolution products can be found in the Appendix B. The spatial distribution of the considered index during the focus period is an essential information if the aim is to spot where irrigation actually occurs. In fact, by considering the mean value inside the two pilot irrigation areas only could be misleading, because it is not always true that all the irrigable land is actually irrigated.

The maps derived from the SURFEX-ISBA modeled soil moisture can be considered as a reference for a situation not taking into account of irrigation. In the LSM, the spatial distribution of surface soil moisture responds to precipitation events and it is mainly governed by soil texture and vegetation cover. For the focus period in 2016, the mean relative difference calculated for the downscaled products reproduces well the contrast between the irrigation districts and the dryland at East of the Urgell. During the focus period in 2017, SMAP at 1 km provides positive values of the relative differences within both the irrigation areas, while SMOS at 1 km shows bad performances for the Urgell. The relative differences retrieved from Sentinel-1 soil moisture reproduce well only the upper part of the dryland at East of the irrigated area, where rainfed croplands are located; negative relative differences are obtained for the Urgell, while positive relative differences can be detected in the central part of the Catalan and Aragonese domain.

4.1.2. Temporal anomalies

The second index used in this study to evaluate the capability of several microwave soil moisture products to detect irrigation is the temporal anomaly, which quantifies how much the soil moisture in a certain observation day differs from the temporal mean, calculated in this case for the whole study period. Fig. 4 shows the time series of the 7-days moving average referred to the mean value of the temporal

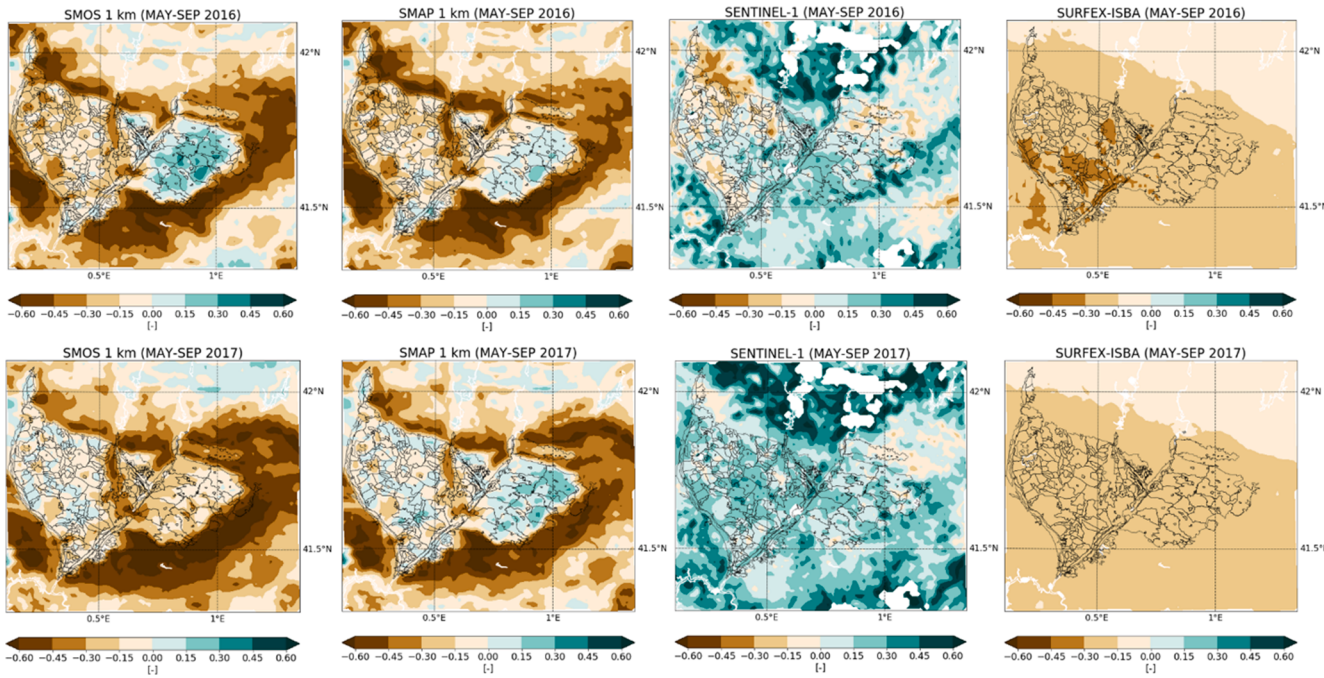


Fig. 5. Maps of the temporal anomalies averaged during the periods May–September 2016 (upper panel) and May–September 2017 (lower panel).

anomalies calculated for the Urgell area, for the Catalan and Aragonese area, and for the dryland; for each product, the same colour has been kept for time series referred to the three areas.

The analysis in terms of temporal anomalies allows looking at the temporal dynamics of soil moisture, thus not considering the influence of static patterns, e.g. soil texture, that may affect soil moisture observations. Good performances in detecting irrigation are represented by higher anomalies within the districts than over the surrounding area during the irrigation period. The downscaled products show mean values of the temporal anomalies for the irrigable areas higher than those calculated for the dryland during both focus periods (except for SMOS at 1 km in the Urgell domain during the period May–September 2017). Sentinel-1 shows positive temporal anomalies over the irrigable land, but this behaviour is probably not attributable to the irrigation, as similar patterns can be observed over the dryland as well; hence, the different wetness conditions coexisting in the pilot area are not detected. Finally, the time series of the temporal anomalies derived from the coarser resolution soil moisture products adopted in this study over the irrigation districts do not show clear discrepancies with respect to the time series referred to the dryland. As stated before, to make evaluations only by looking at the areal mean value can lead to missing information about the actual spatial occurrence of irrigation, so maps of the temporal anomalies averaged for the periods May–September 2016 and 2017 are provided (Fig. 5). In this section, only the maps for the high-resolution data sets are shown; the maps referred to the coarser resolution products can be found in the Appendix B.

For the downscaled products, the anomalies within the irrigable area are higher than over the surrounding dryland and are often greater than or equal to zero, as expected. Furthermore, during both the focus periods, a homogeneous pattern of positive temporal anomalies over the Urgell domain can be observed (except for SMOS at 1 km in the period May–September 2017). During the focus period in 2016, the anomalies obtained by SMOS and SMAP at 1 km rarely are higher than zero over the Catalan and Aragonese area, while in the focus period in 2017 positive values can be observed. However, over this area the anomalies are higher than over the dryland. The Sentinel-1 retrieved soil moisture product shows an unexpected behaviour without differences between the spatial anomalies distributions inside and outside the irrigable areas, corroborating previously described results. Finally, the maps obtained

Table 1

Description of the sixteen different parameters combinations adopted to perform the clustering.

Reference period: MAY-SEPTEMBER 2016		
Code	Input parameters	Category
ST.A. SMOS16	$\sigma(\delta_x)$, \bar{A}_x from SMOS at 1 km	Satellite soil moisture based
ST.A. SMAP16	$\sigma(\delta_x)$, \bar{A}_x from SMAP at 1 km	
D.A.SMOS16	$\bar{\delta}_x$, \bar{A}_x from SMOS at 1 km	
D.A.SMAP16	$\bar{\delta}_x$, \bar{A}_x from SMAP at 1 km	
ST.A.C. SMOS16	$\sigma(\delta_x)$, \bar{A}_x , r_x from SMOS at 1 km	Merging modeled and remotely sensed soil moisture
ST.A.C. SMAP16	$\sigma(\delta_x)$, \bar{A}_x , r_x from SMAP at 1 km	
D.A.C. SMOS16	$\bar{\delta}_x$, \bar{A}_x , r_x from SMOS at 1 km	
D.A.C. SMAP16	$\bar{\delta}_x$, \bar{A}_x , r_x from SMAP at 1 km	
Reference period: MAY-SEPTEMBER 2017		
Code	Input parameters	Category
ST.A. SMOS17	$\sigma(\delta_x)$, \bar{A}_x from SMOS at 1 km	Satellite soil moisture based
ST.A. SMAP17	$\sigma(\delta_x)$, \bar{A}_x from SMAP at 1 km	
D.A.SMOS17	$\bar{\delta}_x$, \bar{A}_x from SMOS at 1 km	
D.A.SMAP17	$\bar{\delta}_x$, \bar{A}_x from SMAP at 1 km	
ST.A.C. SMOS17	$\sigma(\delta_x)$, \bar{A}_x , r_x from SMOS at 1 km	Merging modeled and remotely sensed soil moisture
ST.A.C. SMAP17	$\sigma(\delta_x)$, \bar{A}_x , r_x from SMAP at 1 km	
D.A.C. SMOS17	$\bar{\delta}_x$, \bar{A}_x , r_x from SMOS at 1 km	
D.A.C. SMAP17	$\bar{\delta}_x$, \bar{A}_x , r_x from SMAP at 1 km	

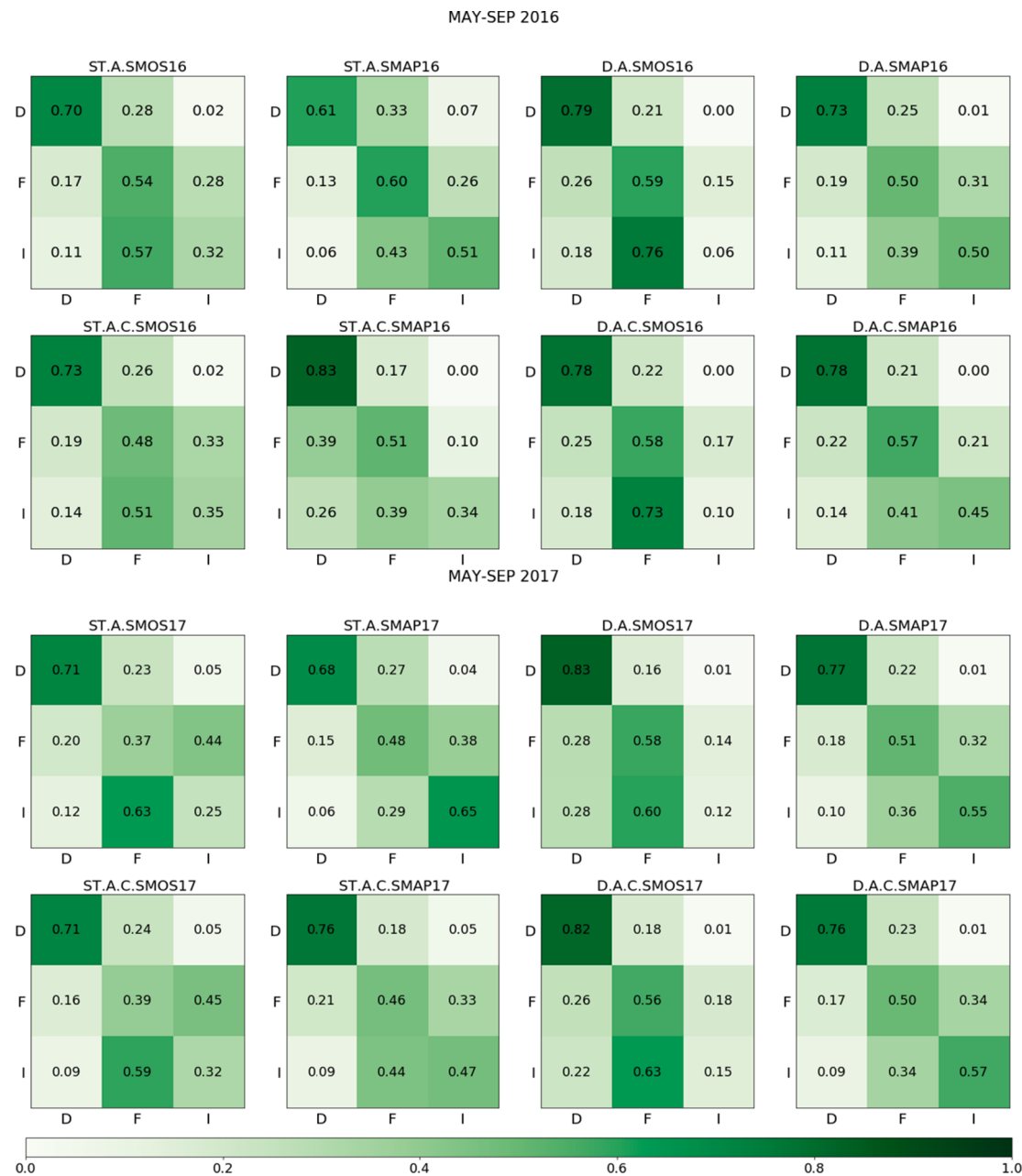


Fig. 6. Confusion matrices related to the first validation of the classification of dryland (D), forest or natural areas (F), and irrigated land (I) for each combination of the input parameters during the periods May–September 2016 (upper panel) and 2017 (lower panel). The ground truth classes are represented on the Y-axis, while the clustering-derived classes are shown on the X-axis.

from the modeled soil moisture data set still show a uniform, dry situation, which is expected during summer from a modeled data set does not taking into account of irrigation.

4.2. Classification based on the K-means algorithm

On the basis of the previously described results, the analysis has been refined. The best performing products, SMOS and SMAP at 1 km, have been exploited to map the irrigated areas through the K-means clustering algorithm. Three clusters representing the three classes of natural surfaces detectable in the study area have been considered: the actually irrigated area, the dryland, and the forest or natural areas. The clustering has been performed by merging information from satellite retrieved and modeled soil moisture. It does not require training processes and is based on the statistic and temporal stability derived

features that are expected to show a clear behaviour over the irrigated areas during the focus periods. The input parameters of the clustering are the mean temporal anomaly, \bar{A}_x , the mean relative difference, $\bar{\delta}_x$, the standard deviation of relative differences, $\sigma(\delta_x)$, and the correlation with the model, r_x (further details on the correlation analysis can be found in Appendix C); the first two parameters are expected to assume higher values over the irrigated areas, while the latter two are expected to show lower values over the same domain. All the parameters have been calculated for both the focus periods considered in this study. The information from the modeling has been involved in the clustering in order to evaluate whether it can bring benefits with respect to considering remotely sensed data only for the mapping of irrigation. Table 1 describes the eight combinations of input parameters used to generate an equal number of maps for each focus period, May–September 2016 and 2017, for a total of sixteen maps. It is noteworthy that the performed

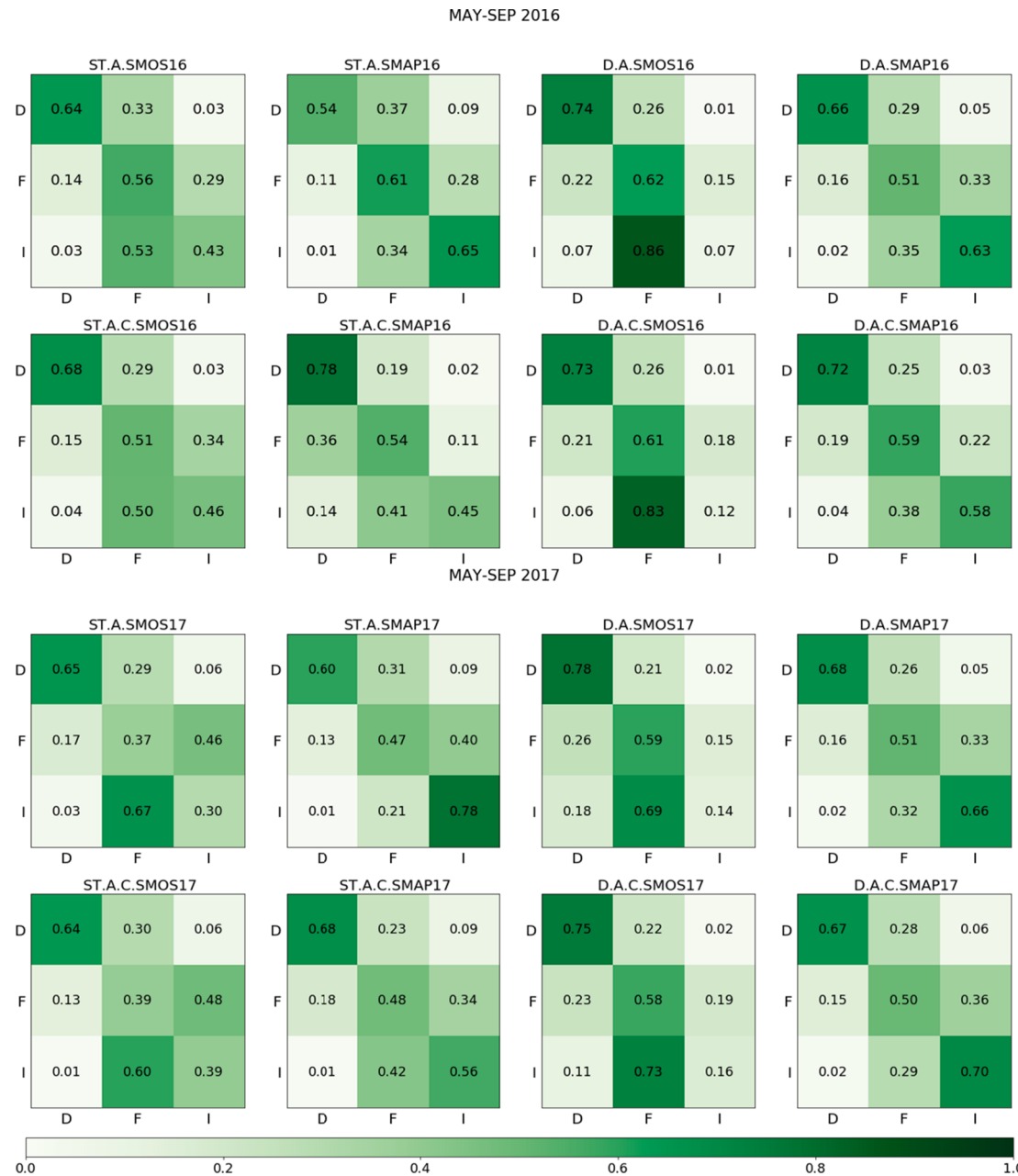


Fig. 7. Confusion matrices related to the second validation of the classification of dryland (D), forest or natural areas (F), and irrigated land (I) for each combination of the input parameters during the periods May–September 2016 (upper panel) and 2017 (lower panel). The ground truth classes are represented on the Y-axis, while the clustering-derived classes are shown on the X-axis.

classifications can be grouped into two main categories: one exploiting satellite soil moisture only (clustering with two input parameters and three clusters) and the other merging information from modeled and remotely sensed soil moisture (clustering with three input parameters and three clusters).

The resulting maps have been validated in two different configurations and results are shown in the next sections.

4.2.1. First validation procedure

In the first validation, the maps have been compared with those obtained from the ground truth data set by exploiting the information about the irrigation coefficient; SIGPAC derived maps of dryland (D, corresponding to non-irrigated fields), irrigated areas (I, corresponding to irrigated fields) and forest or natural areas (F, corresponding to the remaining areas) have been compared with the clustering classification

maps. Before the validation, the data outside the spatial availability of the ground truth data set (Catalonia) have been masked out, as well as the urban areas and the inland water bodies. Fig. 6 shows the confusion matrices resulting from comparisons between the ground truth and the performed classifications. Each matrix is referred to a specific classification identified by the combination of the input parameters used; the ground truth classes are represented on the Y-axis, while on the X-axis the classes derived from the clustering process are shown. The more a classification reproduces the ground truth, the higher values on the diagonal of the matrix and lower values outside can be observed.

During the period May–September 2016, all the performed classifications reproduce well the dryland; in fact, the percentage of dryland pixels well classified through the K-means algorithm ranges between 61% and 83% of the total dryland pixels. Lower scores are observed for the forest or natural areas and for the irrigated areas, which in several

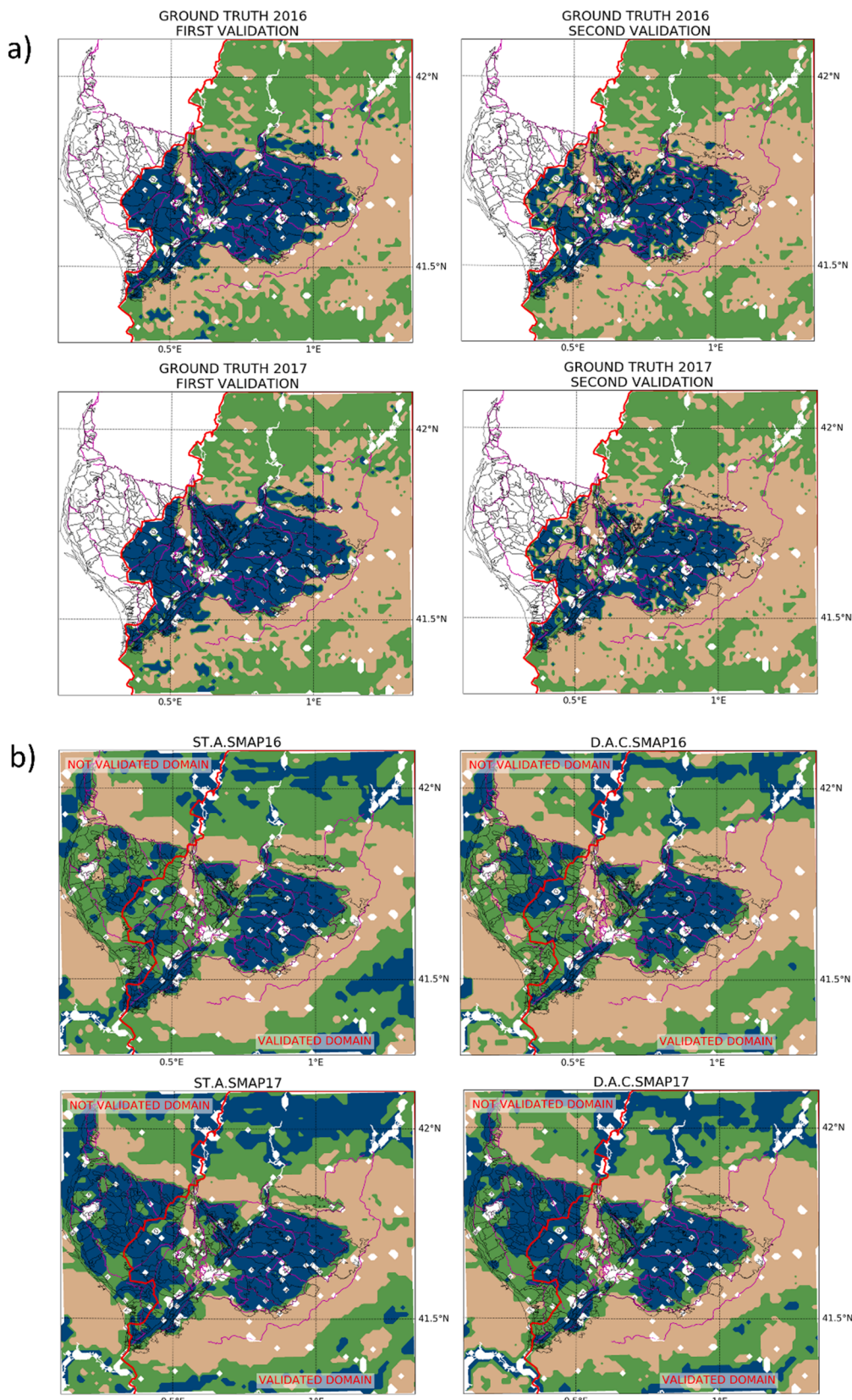


Fig. 8. Ground truth (a) and clustering derived (b) maps for the periods May-September 2016 and May-September 2017. The irrigated areas are represented in blue, the forest or natural areas in green and the dryland in brown. (For interpretation of the references to colour in this figure legend, the reader is referred to the web version of this article.)

experiments are wrongly classified. However, in the classification identified by the code ST.A.SMAP16, the percentages of natural and irrigated areas well classified reach the values of 60% and 51%, respectively. It can also be observed that SMAP at 1 km provides overall better classification results; in fact, matrices referred to this product use to show the higher values along the diagonal. It is noteworthy that the percentages of non-irrigated agricultural pixels confused with those irrigated are always low, ranging from 0% to 7% and equal to 0% according to four classifications. The same is valid by looking at the confusion between the irrigated and the not irrigated areas, ranging between 6% and 26%. This result highlights that the method performs well in distinguishing the irrigated areas from those not irrigated. During the focus period in 2017, a similar behaviour can be observed. Also in this case, the dryland is well reproduced, with percentages ranging between 68% and 83%. Confusion between forest and irrigated areas still persist, even if with the classification ST.A.SMAP17 the 65% of the ground truth irrigated pixels are well classified by the proposed method and in the experiment D.A.SMOS17 the 58% of the forest or natural pixels obtained by the SIGPAC data are well reproduced by the clustering. The overall better performances of classifications based on data from SMAP at 1 km are confirmed, as well as the capability of the method to separate the irrigated areas from those not irrigated. The percentage of the pixels belonging to the dryland class that are misinterpreted as irrigated from the clustering ranges between 1% and 5%, while the percentage referred to irrigated pixels confused with those not irrigated ranges between 6% and 28%.

4.2.2. Second validation procedure

A second validation of the clustering derived maps has been performed by exploiting another kind of information from the ground truth data set. Instead of the information regarding the irrigation coefficient, the one linked to the kind of crops has been used. This alternative validation, which is specific for summer crops, is driven by the consideration that it may happen that a certain plot has the irrigation attribute associated to it because it is capable to reach the irrigation network but this does not imply that has been actually irrigated during the reference period for which the clustering maps have been produced, that is May–September. From the perspective of this alternative proposed validation, SIGPAC derived maps of selected summer crops (summer cereals, forage, and fruit trees), other crops, and remaining areas have been interpreted as irrigated areas (I), dryland (D) and forest or natural areas (F), respectively. These maps have been used to perform an alternative validation of the K-means clustering derived maps, whose resulting confusion matrices are shown in Fig. 7.

The results of this second validation show, for both the focus periods, a systematic enhancement of the representation of the forest and of the actually irrigated areas associated with a slight worsening of the detection of the not irrigated areas. However, the percentage of dryland pixels recognized varies between 54% and 78% for the focus period in 2016 and between 60% and 78% for the focus period in 2017. The highest percentage of pixels belonging to the forest or natural areas class well detected is equal to 62% in 2016 and to 59% in 2017; both results are referred to the same experiment configuration (D.A.SMOS16 for 2016 and D.A.SMOS17 for 2017). The best performances in detecting the irrigated crops during the focus periods are obtained for the experiments ST.A.SMAP16 in 2016 (percentage of recognized pixels: 65%) and ST.A.SMAP17 (percentage of recognized pixels: 78%).

Also this second validation highlights overall better performances when using data retrieved from SMAP at 1 km. Another common aspect between the two proposed validations is the almost total absence of confusion between irrigated and agricultural non-irrigated areas. The percentage of dryland pixels confused with irrigated pixels ranges between 1% and 9% during the focus period in 2016 and between 2% and 9% during the same period in 2017. Irrigated pixels confused with dryland ones are between 2% and 14% of the total during May–September 2016 and between 1% and 18% during May–September

2017. Finally, not negligible rates of irrigated pixels wrongly classified as natural pixels still persist.

4.2.3. Best performing classifications

According to both the validation procedures presented in this study, the best performing classifications result to be the same, and are shown in Fig. 8. For each year, two classifications have been chosen: the one that overall best reproduces the irrigated areas, represented by the combination ST.A.SMAP16 for 2016 and ST.A.SMAP17 for 2017, and the one that shows the best performances by considering all the three classes concurrently, represented by D.A.C.SMAP16 for 2016 and D.A.C.SMAP17 for 2017. The classes are identified by different colors, blue for the actually irrigated areas, green for the forest or natural areas and brown for the dryland. Together with the classification derived maps, the ground truth maps are also represented. The cities and the inland water areas have been masked out, while the irrigation canals network is represented in magenta. It is noteworthy that the SIGPAC crops maps are available for Catalonia only (East of the red border), so it has not been possible to quantitative validate the K-means clustering derived maps for the portion of the study area falling into Aragon. The overall capability of the method to reproduce the ground truth conditions can be immediately observed, even if the proposed maps show some disturbances due to a system of reservoirs in the North of the study area and to evergreen forests in the South-East.

5. Discussion

This study investigates the capability of five remotely sensed soil moisture products to detect the irrigation signal over an intensely irrigated area located in the North East of Spain; in addition, a method to classify and map irrigated areas is proposed. The evaluation of the performances of the satellite products in detecting the irrigated areas has been addressed by looking at the spatial and temporal dynamics of soil moisture through normalized indices derived from the temporal stability theory. According to all the performed analyses, the enhanced resolution L-band passive microwave based products result to be the most skilful ones in detecting irrigation over the study area. Analyses based on the relative differences, revealing the spatial dynamics of soil moisture, indicate SMAP at 1 km as the data set showing the clearest irrigation signal over the Urgell area, while SMOS at 1 km results the best performing product over the Catalan and Aragonese area according to the same metric. Analyses based on the temporal anomalies, which allow to investigate the temporal dynamics of soil moisture, reveal a clear pattern of positive anomalies over the Urgell area during the focus period in 2016 for both SMOS and SMAP at 1 km. This area is where flood irrigation is the most widespread technique. During May–September 2017, the results obtained for the downsampled products over the Urgell area are not comparable, because of a RFI source detected in this area since the end of 2016 onwards (see Appendix D); however, over the Catalan and Aragonese area, the products show a similar behaviour. Sentinel-1 is unable to reproduce well the spatial distribution of the different wetness conditions coexisting in the study area. Moreover, the analysis in terms of temporal anomalies reveals unexpected uniform wetness conditions during the dry season. The unsatisfactory performances obtained with Sentinel-1 can be explained by the higher sensitivity to vegetation and surface roughness characterizing the C-band active sensors with respect to the L-band passive sensors; in addition, the non-implementation of a correction for seasonal vegetation effects in the retrieval algorithm (Bauer-Marschallinger et al., 2018) can represent a complementary reason for the poor performances of Sentinel-1 over the pilot area. The coarser resolution products adopted in this study, ASCAT and SMAP, do not show promising results in detecting irrigation over the pilot area. This issue can be attributed to the scale of the irrigated land and to the complexity of the surrounding landscape with respect to the resolution of the products, too coarse to capture the differences existing at the considered scale. Both products, in

fact, proved to be capable to detect irrigation signal over different wide irrigated areas in the continental United States (Kumar et al., 2015; Lawston et al., 2017). The downscaling through optical data from MODIS represents an enhancement making the DISPATCH downscaled products suitable for obtaining reliable spatial information about irrigated areas where high resolution is needed. The potential of SMOS at 1 km in detecting irrigation occurring over the pilot area was already shown in (Escorihuela and Quintana-Seguí, 2016); nevertheless, in that study the authors compared remote sensing and modeled soil moisture over different land covers, finding inconsistencies over irrigated areas attributed to the irrigation occurrence. In this work, an analysis involving three high-resolution products and specifically focused on the irrigation detection by using diagnostic indices derived from the temporal stability theory is presented. In addition, a method to map irrigated areas based on a K-means clustering classification and exploiting the downscaled data sets is proposed. Despite many existing classification methods require training processes and rules based on decision tree structures (Thenkabail et al., 2007; Ozdogan and Gutman, 2008; Jin et al., 2016; Teluguntla et al., 2017), the method proposed in this study does not require any training; in fact, it is based on indices obtained from remotely sensed soil moisture that are expected to assume a clear and distinct behaviour over irrigated areas and over the other kinds of surfaces. From both the validation procedures carried out, it appears clear how the method is able to separate irrigated areas from not irrigated agricultural areas, thus representing a useful tool to retrieve the actually irrigated portion of areas that are known to be equipped for irrigation. By looking at the best resulting classification maps shown in Fig. 8 and at their related confusion matrices in Figs. 6 and 7, recurring confusion between forest or natural areas and irrigated areas can be observed. The percentages of forest or natural pixels confused with those irrigated can be mainly attributed to the system of reservoirs located in the North of the study area and feeding the irrigation canals network, which alter the soil wetness conditions retrieved from the satellite products. Conversely, the percentages of irrigated pixels confused with forest or natural areas can be mainly attributed to the difficulty of the method to correctly distinguish between areas where fruit trees are cultivated and highly mixed areas, like the upper part of the Urgell, where isolated corn crops, abandoned fields and fruit trees fields coexist. However, the fact that the proposed method interprets this kind of areas as natural land is important and valuable. Difficulties in the correct classification of fruit trees areas were also found in Gao et al. (2018). Fruit trees are usually drip irrigated, a very localized irrigation method that is difficult to detect using remote sensing soil moisture data; consequently, over this kind of areas the soil moisture might assume lower values than over areas destined to other irrigated crops, thus leading to a wrong classification during the clustering. The above discussed best performing classifications are obtained by exploiting SMAP at 1 km data set, which performs better than SMOS at 1 km in the clustering. The higher accuracy of coarse resolution SMAP data with respect to coarse resolution SMOS data is supported by several validation studies (e.g., Chen et al., 2018). However, the DISPATCH downscaled versions of SMOS and SMAP at 1 km are both skilful in detecting irrigation over the study area, but the SMOS-derived clustering experiments are influenced by the RFI problems described in Appendix D. Finally, it is noteworthy that the adoption of less restrictive thresholds when aggregating the ground truth data to a coarser resolution can lead to an improvement of the performances of the already well performing combinations; conversely, this gain is not observed for already bad performing combinations (see Appendix A).

6. Conclusions

On the basis of the above discussed results, the main findings of this study can be summarized as follows:

- 1) the spatial scale of the irrigation processes and the complexity of the study area make necessary the adoption of high-resolution (1 km or less) soil moisture products to detect the irrigation signal;
- 2) indices derived from the temporal stability theory represent useful tools to investigate both spatial and temporal dynamics of soil moisture and to evaluate the capability of remotely sensed soil moisture to detect irrigated areas;
- 3) SMOS and SMAP at 1 km (DISPATCH downscaled) proved to be the most suitable products to detect irrigation over the pilot area;
- 4) the proposed irrigation mapping method performs well in separating irrigated areas from agricultural rainfed areas. The percentages of ground truth dryland pixels confused with irrigated pixels range between 0% and 9%. The irrigated pixels wrongly classified as dryland range between 1% and 28%, but percentages higher than 20% can be observed for the first validation method proposed only;
- 5) for both the focus periods, the best resulting classification are the same and the best performing product is SMAP at 1 km; the combinations ST.A.SMOS16 and ST.A.SMOS17 are those that overall best represent irrigated areas. It is noteworthy that these combinations exploit remotely sensed data only, meaning that the model does not add information for mapping irrigation. This is comforting if we consider the scarcity of models running at 1 km over large regions;
- 6) the experiments identified by the combinations D.A.C.SMOS16 and D.A.C.SMOS17 are those that overall best represent the three considered classes concurrently and merge information from satellite and modeled soil moisture.

The capability of the L-band passive microwave downscaled products to detect irrigation and the correct distinction between areas where irrigation actually occurs and agricultural rainfed areas achieved by the proposed method constitute a solid basis for studies aimed to quantify the amounts of irrigation water. In addition, the assessment of the potential in producing maps of irrigated areas at a very high spatial resolution through the proposed methodology with plot-scale resolution soil moisture data (e.g., from Sentinel-1) as input is among the future perspectives of this study.

CRediT authorship contribution statement

Jacopo Dari: Conceptualization, Methodology, Software, Validation, Formal analysis, Investigation, Writing - original draft, Writing - review & editing, Visualization. **Pere Quintana-Seguí:** Conceptualization, Methodology, Validation, Writing - review & editing. **María José Escorihuela:** Validation, Writing - review & editing, Supervision. **Vivien Stefan:** Validation, Writing - review & editing, Supervision. **Luca Brocca:** Conceptualization, Methodology, Writing - review & editing, Supervision. **Renato Morbidelli:** Conceptualization, Methodology, Writing - review & editing, Supervision.

Declaration of Competing Interest

The authors declare that they have no known competing financial interests or personal relationships that could have appeared to influence the work reported in this paper.

Acknowledgments

The authors acknowledge the support from ESA under the IRRIGATION + project (contract n. 4000129870/20/I-NB). The authors wish to thank the SIGPAC team for providing the ground truth data used in this study.

Appendix A. . Sensitivity of the classification to the aggregation threshold

It is well known that the aggregation to coarser resolutions produces a loss of information. In order to test the sensitivity of the performed classifications to this issue, two data sets containing binary information linked to the ground truth data used to perform the validations described in the section 3.6.2 have been derived. The two data sets contain only the irrigated crops and only the summer crops, respectively, inside the irrigated areas. The procedure to obtain these products at 1 km consists in projecting the data on a 100 m resolution regular grid as a first step and then in aggregating it to the 1 km grid by assigning to the $1 \text{ km} \times 1 \text{ km}$ pixel the class irrigated (or summer crops) if the pixels at $100 \text{ m} \times 100 \text{ m}$ contained in it are more than the 30%, 40%, 50% and 60% of the total. This aggregation technique allows to obtain sixteen additional ground truth data set, eight for 2016 and eight for 2017, with information about the irrigated pixels only and the selected summer crops only, obtained by considering four different aggregation thresholds (0.3, 0.4, 0.5 and 0.6).

The results of the assessment of the sensitivity to the aggregation threshold when aggregating the benchmark ground truth data to the coarser 1 km resolution are shown in Fig. A.1. For both the validation procedures adopted in this study, it can be observed that for the well performing classifications the percentage of pixels with the irrigation (or summer crops) information that are well represented by the proposed method increases when the aggregation threshold increases, even reaching the 90% when a threshold of 0.6 is considered. Conversely, changes in the considered aggregation threshold do not enhance the worst performing classifications. This is a simplified experiment, in which the distinction is made only between two and not three classes, but it gives an idea of the partial loss of information occurring when the ground truth data is aggregated to the remote sensing products resolution and it confirms the capability of the method to well interpret homogeneous irrigation pattern.

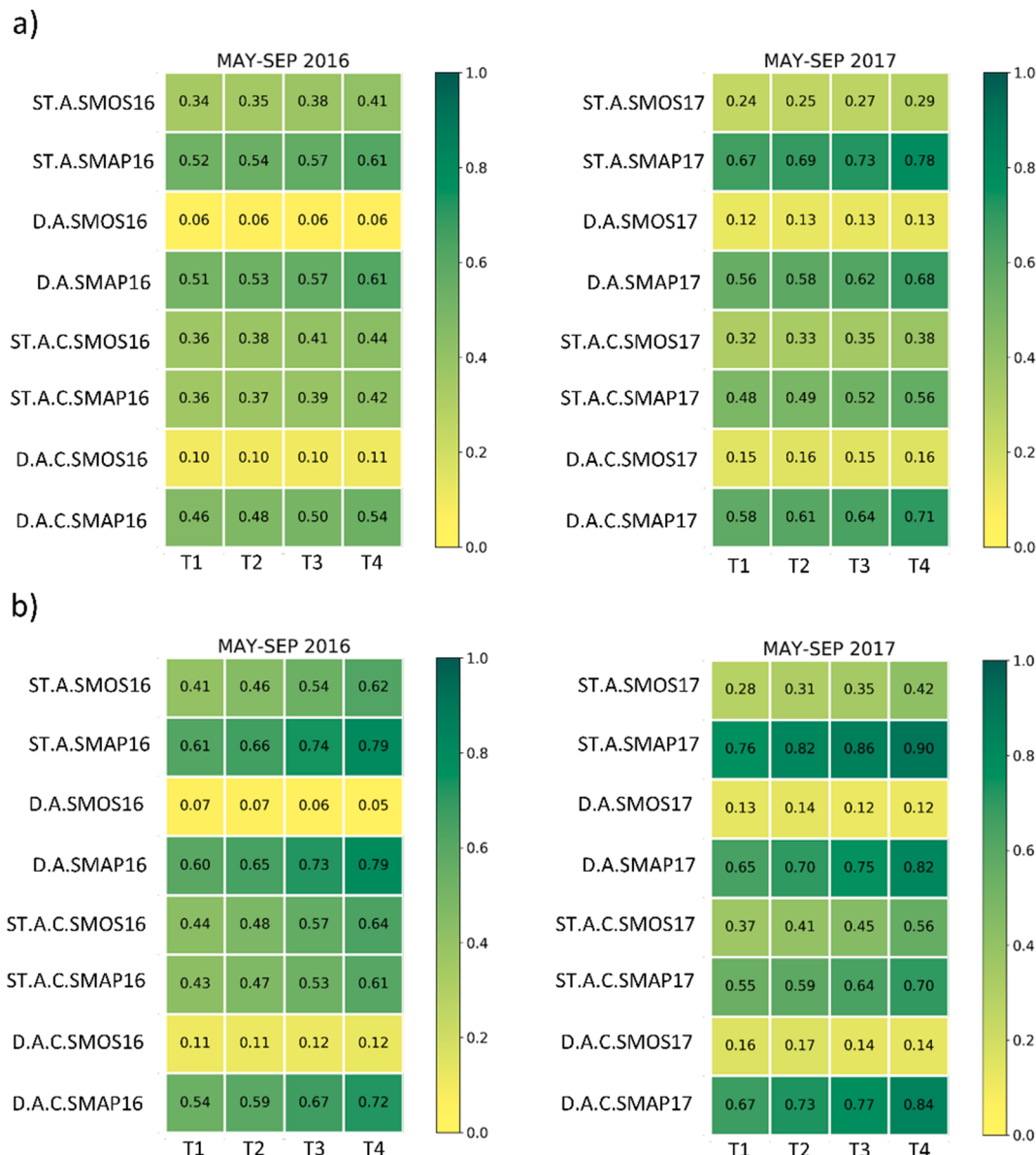


Fig. A1. Heatmaps representing the classification accuracy of the irrigated pixels at different aggregation thresholds ($T1 = 0.3$, $T2 = 0.4$, $T3 = 0.5$, $T4 = 0.6$) considering: a) all the pixels inside the irrigable land marked as irrigated in the ground truth data set (SIGPAC) and b) only the pixels in the same domain carrying the information about the selected summer crops.

Appendix B. . Maps of temporal stability derived indices for the coarser resolution products

For complete information, the maps of the temporal stability indices calculated for the coarser resolution products used in this study are shown.

[Fig. B.1](#) shows the maps of the spatial relative differences calculated for the coarser resolution products (SMAP and ASCAT) and averaged during both focus periods considered in this study. [Fig. B.2](#) shows the maps of the temporal anomalies obtained from the same products and averaged during the same periods.

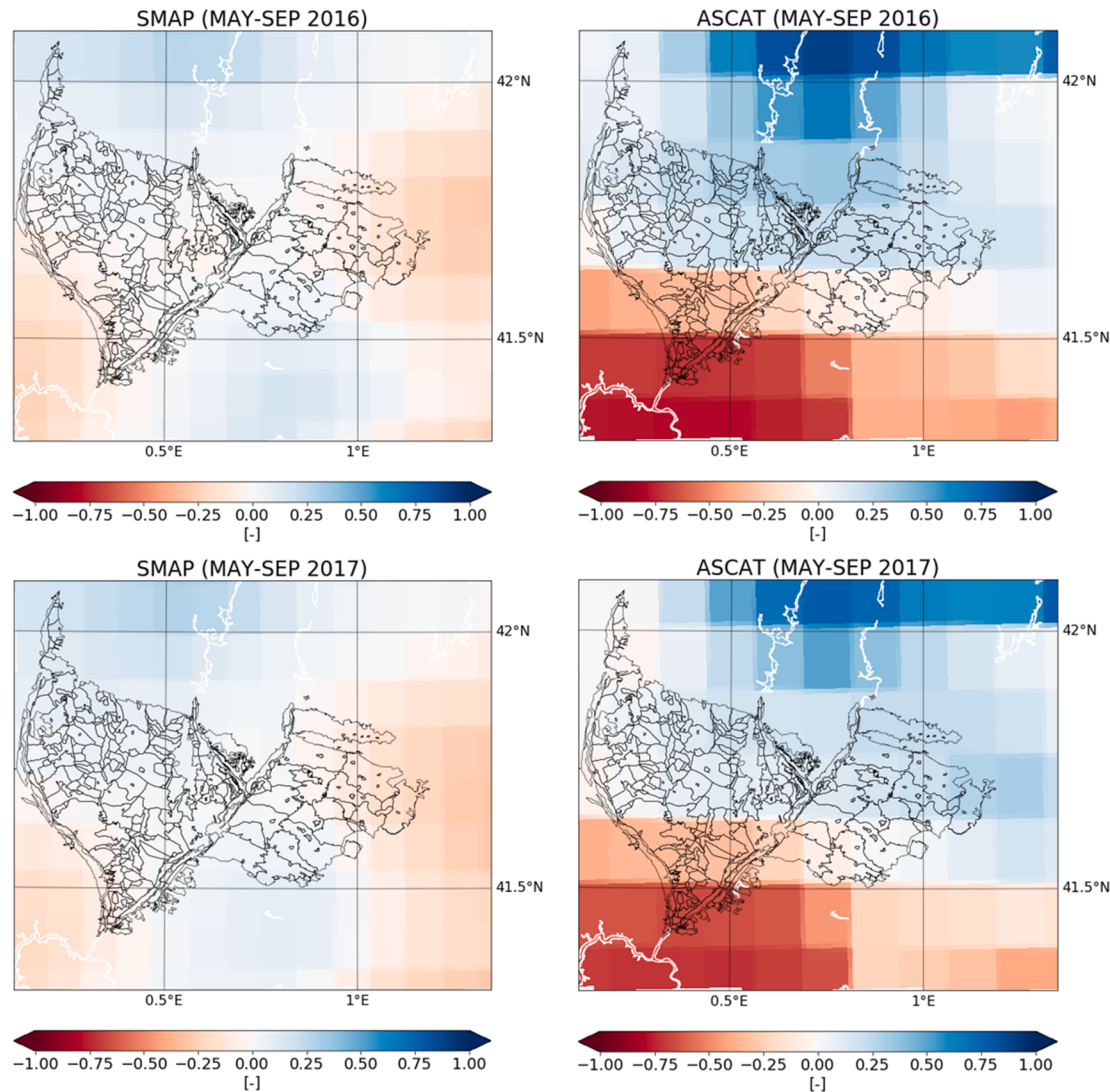


Fig. B1. Maps of the spatial relative differences referred to the coarser resolution products and averaged during the periods May–September 2016 (upper panel) and May–September 2017 (lower panel).

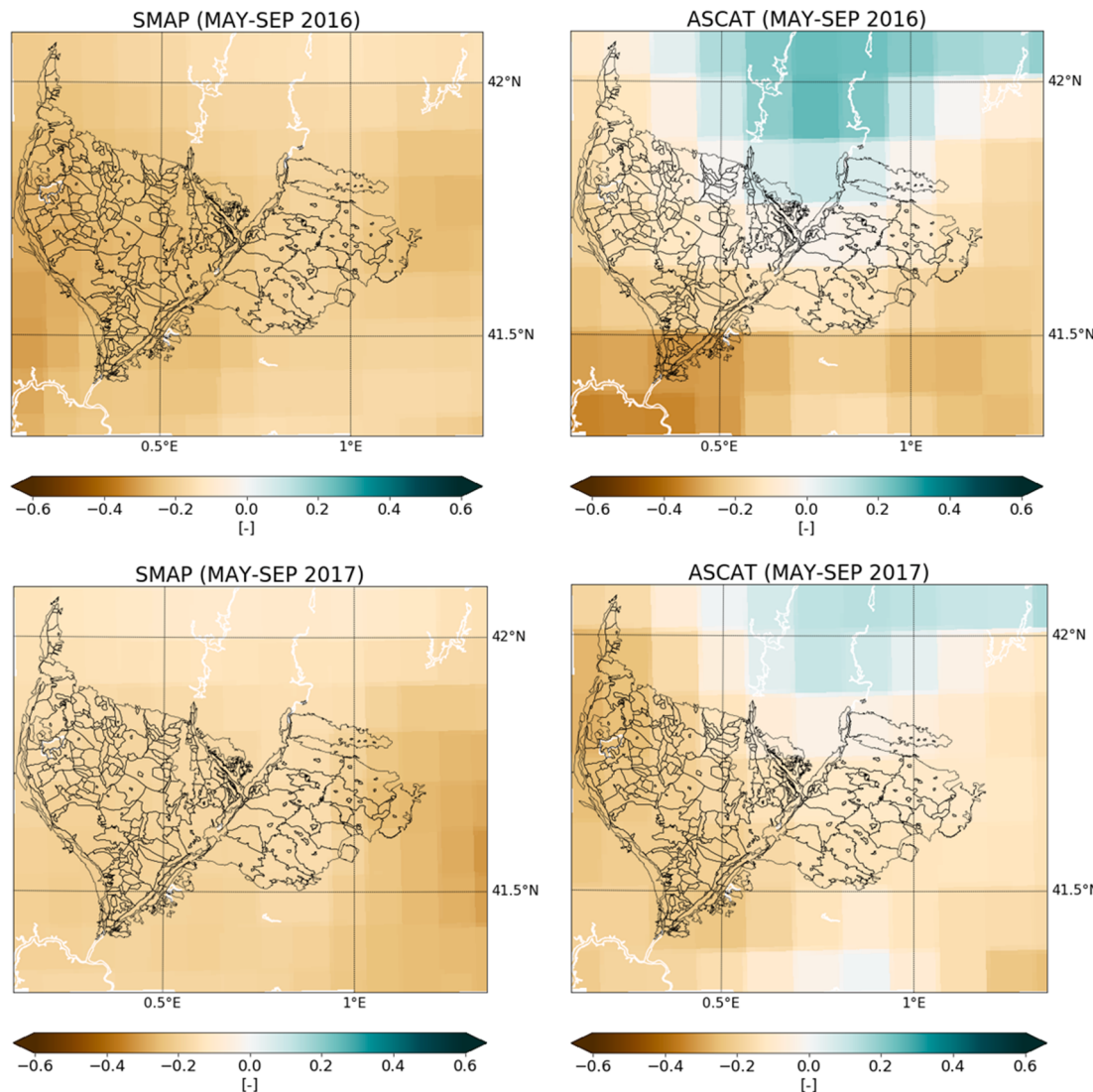


Fig. B2. Maps of the temporal anomalies calculated for the coarser resolution products and averaged during the periods May–September 2016 (upper panel) and May–September 2017 (lower panel).

Appendix C. . Correlation analysis

The correlation between the time series of remotely sensed and modeled soil moisture is a statistical feature that can be used to evaluate the detectability of irrigation over the pilot area (Escorihuela and Quintana-Seguí, 2016). To this aim, the correlation between remotely sensed soil moisture data sets (SMOS and SMAP at 1 km) and the modeled one during the irrigation seasons in 2016 and 2017 has been investigated. Fig. C.1 shows the spatial distribution of the Pearson correlation coefficient (r_x) calculated for the DISPATCH downscaled soil moisture products against SURFEX-ISBA soil moisture. The modeled soil moisture does not take irrigation into account, so, by assuming that precipitation is correct, low (scarce correlation) or negative (inverse correlation) r_x values within an irrigated area can be an indicator of the remotely sensed product capability to contain the irrigation information.

The downscaled products show similar behaviours; in the period May–September 2016, both SMOS and SMAP at 1 km show a clear pattern of low correlation in the upper and central zones of the irrigation areas. Outside the irrigable lands the correlation rises. During May–September 2017, the irrigation-related pattern is less clear, but over the irrigable land correlation lower than over the dryland (especially over the rainfed cropland, in the upper part) can still be observed.

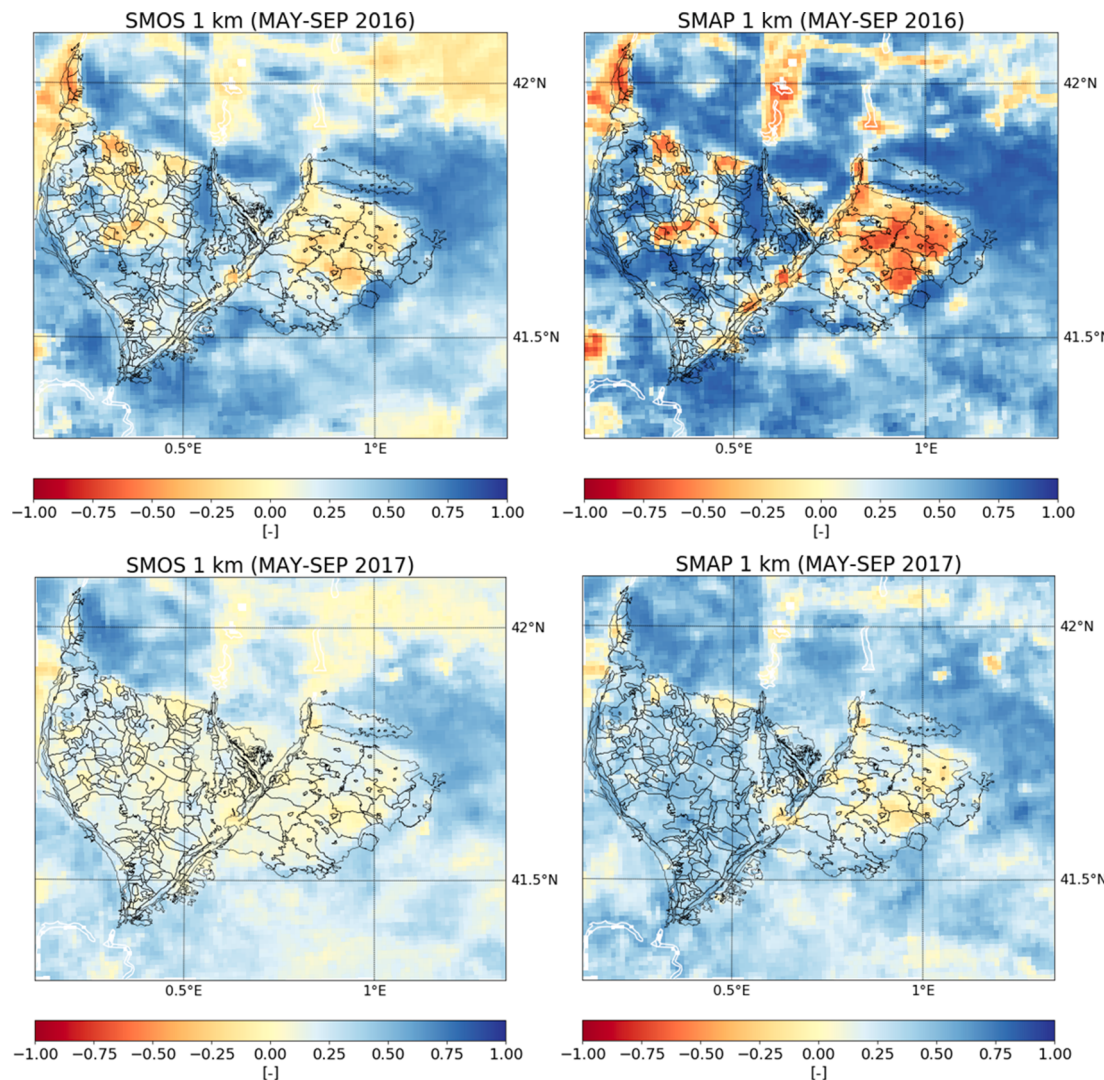


Fig. C1. Maps of the correlation between the satellite products used in the clustering experiments and modeled soil moisture for the periods May–September 2016 (upper panel) and May–September 2017 (lower panel).

Appendix D. . RFI problems affecting SMOS data in 2017

During the period May–September 2017, SMOS at 1 km shows an anomalous behaviour over the Urgell, especially if compared with the performances over the same area in 2016 and over the Catalan and Aragonese area during both focus period, which are generally in agreement with those shown by the other downscaled product, SMAP at 1 km. This issue is due to a source of RFI detected over the Urgell area and not correctly solved by the post-processing through the RFI filter. Fig. D.1 shows the probability of RFI occurrence in the Urgell area. In the second part of the 2016, the RFI probability begins rising, reaching values close to 0.7 in 2017. As a result, the dielectric constant of the soil and thus the soil wetness conditions are underestimated. This problem does not affect the other downscaled product considered in this study, SMAP at 1 km. The SMAP radar and radiometer electronics and algorithms are more recent than the SMOS mission, and have been designed to include on board filters to mitigate RFI effects (Entekhabi et al., 2010).

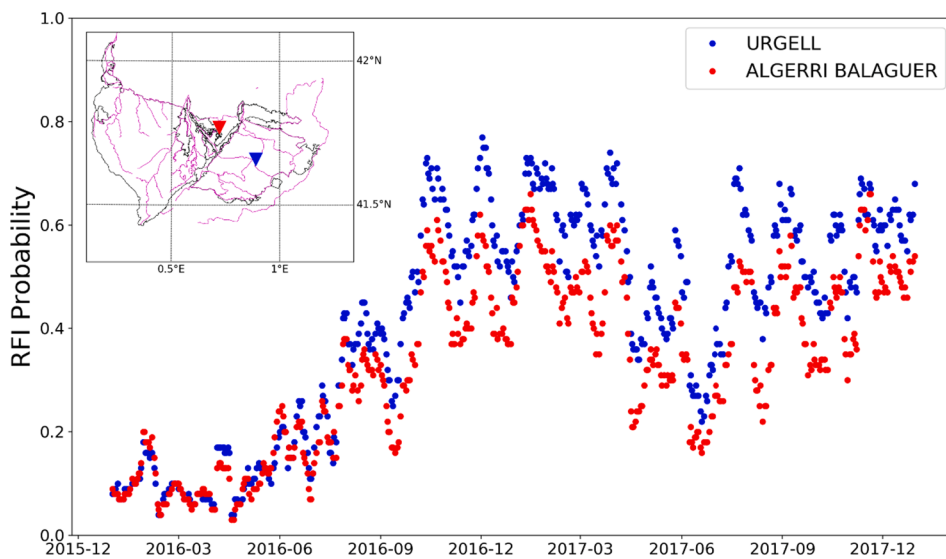


Fig. D1. Time series of the RFI probability referred to two locations: Algerri-Balaguer (red) and Urgell (blue). (For interpretation of the references to colour in this figure legend, the reader is referred to the web version of this article.)

References

- Albergel, C., Dutra, E., Munier, S., Calvet, J.C., Muñoz-Sabater, J., de Rosnay, P., Balsamo, G., 2018. ERA-5 and ERA-Interim driven ISBA land surface model simulations: which one performs better? *Hydrol. Earth Syst. Sci.* 22, 3515–3532.
- Alter, R.E., Im, E.S., Eltahir, E.A., 2015. Rainfall consistently enhanced around the Gezira Scheme in East Africa due to irrigation. *Nat. Geosci.* 8, 763–767.
- Ambika, A.K., Mishra, V., 2016. Remotely sensed high resolution irrigated area mapping in India for 2000 to 2015. *Sci. Data* 3, 160118.
- Bartalis, Z., Wagner, W., Naeimi, V., Hasenauer, S., Scipal, K., Bonekamp, H., Figa, J., Anderson, J., 2007. Initial soil moisture retrievals from the METOP-A Advanced Scatterometer (ASCAT). *Geophysical Research Letters*. 34, L20401.
- Bauer-Marschallinger, B., Naeimi, V., Cao, S., Paulik, C., Schaufler, S., Stachl, T., Modanesi, S., Ciabatta, L., Massari, C., Brocca, L., Wagner, W., 2018. Towards global soil moisture monitoring with Sentinel-1: harnessing assets and overcoming obstacles. *IEEE Trans. Geosci. Remote Sens.* 57, 520–539.
- Boone, A., 2000. Modélisation des processus hydrologiques dans le schéma de surface ISBA: Inclusion d'un réservoir hydrologique, du gel et modélisation de la neige. Ph. D. thesis Université Paul Sabatier (Toulouse III).
- Boone, A.A., Calvet, J.C., Noilhan, J., 1999. The inclusion of a third soil layer in a land surface scheme using the force-restore method. *J. Appl. Meteorol.* 38, 1611–1630.
- Brocca, L., Melone, F., Moramarco, T., Morbidelli, R., 2010. Spatial-temporal variability of soil moisture and its estimation across scales. *Water Resour. Res.* 46, W02516.
- Brocca, L., Tarpanelli, A., Filippucci, P., Dorigo, W., Zaussinger, F., Gruber, A., Fernández-Prieto, D., 2018. How much water is used for irrigation? A new approach exploiting coarse resolution satellite soil moisture products. *Int. J. Earth Obs. Geoinf.* 73, 752–766.
- Chan, S.K., Bindlish, R., O'Neill, P., Jackson, T., Njoku, E., Dunbar, S., Chaubell, J., Piepmeier, J., Yueh, S., Entekhabi, D., Collander, A., Chen, F., Cosh, M.H., Caldwell, T., Walker, J., Berg, A., McNairn, H., Thibault, M., Martínez-Fernández, J., Uldall, F., Seyfried, M., Bosch, D., Starks, P., Holifield Collins, C., Prueger, J., van der Velde, R., Asanuma, J., Palecki, M., Small, E.E., Zreda, M., Calvet, J., Crow, W.T., Kerr, Y., 2018. Development and assessment of the SMAP enhanced passive soil moisture product. *Remote Sens. Environ.* 204, 931–941.
- Chen, F., Crow, W.T., Bindlish, R., Collander, A., Burgin, M.S., Asanuma, J., Aida, K., 2018. Global-scale evaluation of SMAP, SMOS and ASCAT soil moisture products using triple collocation. *Remote Sens. Environ.* 214, 1–13.
- Dari, J., Morbidelli, R., Saltalippi, C., Massari, C., Brocca, L., 2019. Spatial-temporal variability of soil moisture: addressing the monitoring at the catchment scale. *J. Hydrol.* 570, 436–444.
- Dari, J., Brocca, L., Quintana-Seguí, P., Escorihuela, M.J., Stefan, V., Morbidelli, R., 2020. Exploiting high-resolution remote sensing soil moisture to estimate irrigation water amounts over a Mediterranean region. *Remote Sens.* 12, 2593.
- Das, N.N., Entekhabi, D., Dunbar, R.S., Chaubell, M.J., Collander, A., Yueh, S., Jagdhuber, T., Chen, F., Crow, W., O'Neill, P.E., Walker, J.P., Berg, A., Bosch, D.D., Caldwell, T., Cosh, M.H., Collins, C.H., Lopez-Baeza, E., Thibault, M., 2019. The SMAP and Copernicus Sentinel 1A/B microwave active-passive high resolution surface soil moisture product. *Remote Sens. Environ.* 233, 111380.
- Druel, A., Albergel, C., Munier, S., Calvet, J.-C., 2019. Implementation of a new irrigation scheme in the ISBA Land Surface Model. EMS Annual Meeting, Copenhagen (Denmark), 9–13 September 2019.
- Entekhabi, D., Njoku, E.G., Neill, P.E., Kellogg, K.H., Crow, W.T., Edelstein, W.N., et al., 2010. The soil moisture active passive (SMAP) mission. *Proc. IEEE* 98 (5), 704–716.
- Escorihuela, M.J., Quintana-Seguí, P., 2016. Comparison of remote sensing and simulated soil moisture datasets in Mediterranean landscapes. *Remote Sens. Environ.* 180, 99–114.
- Filippucci, P., Tarpanelli, A., Massari, C., Serafini, A., Strati, V., Alberi, M., Raptis, K.G. C., Mantovani, F., Brocca, L., 2020. Soil moisture as a potential variable for tracking and quantifying irrigation: a case study with proximal gamma-ray spectroscopy data. *Adv. Water Resour.* 136, 103502.
- Foley, J.A., Ramankutty, N., Brauman, K.A., Cassidy, E.S., Gerber, J.S., Johnston, M., et al., 2011. Solutions for a cultivated planet. *Nature* 478 (7369), 337–342.
- Gao, X., Zhao, X., Si, B.C., Brocca, L., Hu, W., Wu, P., 2015. Catchment-scale variability of absolute versus temporal anomaly soil moisture: time-invariant part not always plays the leading role. *J. Hydrol.* 529, 1669–1678.
- Gao, Q., Zribi, M., Escorihuela, M.J., Baghdadi, N., Quintana-Seguí, P., 2018. Irrigation mapping using Sentinel-1 time series at field scale. *Remote Sens.* 10, 1495.
- Gleick, P.H., 2003. Global freshwater resources: soft-path solutions for the 21st century. *Science* 302, 1524.
- Habets, F., Boone, A., Noilhan, J., 2003. Simulation of a Scandinavian basin using the diffusion transfer version of ISBA. *Glob. Planet. Change* 38, 137–149.
- Hain, C.R., Crow, W.T., Anderson, M.C., Yilmaz, M.T., 2015. Diagnosing neglected soil moisture source-sink processes via a thermal infrared-based two-source energy balance model. *J. Hydrometeorol.* 16, 1070–1086.
- Hersbach, H., Bell, B., Berrisford, P., Hirahara, S., Horányi, A., Muñoz-Sabater, J., Nicolas, J., Peubey, C., Radu, R., Schepers, D., Simmons, A., Soci, C., Abdalla, S., Abellán, X., Balsamo, G., Bechtold, P., Biavati, G., Bidlot, J., Bonavita, M., De Chiara, G., Dahlgren, P., Dee, D., Diamantakis, M., Dragani, R., Flemming, J., Forbes, R., Fuentes, M., Geer, A., Haimberger, L., Healy, S., Hogan, R.J., Hölm, E., Janisková, M., Keeley, S., Laloyaux, P., Lopez, P., Lupu, C., Radnoti, G., de Rosnay, P., Rozum, I., Vamborg, F., Villaume, S., Thépaut, J.-N., 2020. The ERA5 global reanalysis. *Q. J. Roy. Meteor. Soc.* 1–51.
- Hornáček, M., Wagner, W., Sabel, D., Truong, H.-L., Snoeij, P., Hahmann, T., Diedrich, E., Doubková, M., 2012. Potential for high resolution systematic global surface soil moisture retrieval via change detection using Sentinel-1. *Sel. Top. Appl. Earth Obs. Remote Sens.*, IEEE J. Of, 5, 1303–1311.
- Jalilvand, E., Tajrishi, M., Hashemi, S.A.G., Brocca, L., 2019. Quantification of irrigation water using remote sensing of soil moisture in a semi-arid region. *Remote Sens. Environ.* 231, 111226.
- Jin, N., Tao, B., Ren, W., Feng, M., Sun, R., He, L., Zhuang, W., Yu, Q., 2016. Mapping irrigated and rainfed wheat areas using multi-temporal satellite data. *Remote Sens.* 8 (3), 207.
- Kerr, Y.H., Waldteufel, P., Richaume, P., Wigneron, J.P., Ferrazzoli, P., Mahmoodi, A., Al Bitar, A., Cabot, F., Gruhier, C., Juglea, S.E., et al., 2012. The SMOS soil moisture retrieval algorithm. *IEEE Trans. Geosci. Remote Sens.* 50, 1384–1403.
- Kerr, Y.H., Waldteufel, P., Wigneron, J.P., Delwart, S., Cabot, F., Boutin, J., Escorihuela, M.J., Font, J., Reul, N., Gruhier, C., et al., 2010. The SMOS mission: new tool for monitoring key elements of the global water cycle. *Proc. IEEE* 98, 666–687.
- Kerr, Y.H., Waldteufel, P., Wigneron, J.P., Martinuzzi, J.M., Font, J., Berger, M., 2001. Soil moisture retrieval from space: the soil moisture and ocean salinity (SMOS) mission. *IEEE Trans. Geosci. Remote Sens.* 39 (8).
- Kumar, S.V., Peters-Lidard, C.D., Santanello, J.A., Reichle, R.H., Draper, C.S., Koster, R. D., Nearing, G., Jasinski, M.F., 2015. Evaluating the utility of satellite soil moisture retrievals over irrigated areas and the ability of land data assimilation methods to correct for unmodeled processes. *Hydrol. Earth Syst. Sci.* 19, 4463–4478.
- Kummu, M., Guillaume, J., De Moel, H., Eisner, S., Flörke, M., Porkka, M., Siebert, S., Veldkamp, T., Ward, P., 2016. The world's road to water scarcity: shortage and stress in the 20th century and pathways towards sustainability. *Sci. Rep.-UK* 6, 38495.

- Lawston, P.M., Santanello, J.A., Kumar, S.V., 2017. Irrigation signals detected from SMAP soil moisture retrievals. *Geophys. Res. Lett.* 44, 11860–11867.
- MacQueen, J.B., 1967. Some methods for classification and analysis of multivariate observations. Proceedings of 5-th Berkeley Symposium on Mathematical Statistics and Probability, Berkeley, University of California Press, 1, pp. 281–297.
- Mahfouf, J.F.F., Noilhan, J., 1996. Inclusion of gravitational drainage in a land surface scheme based on the force-restore method. *J. Appl. Meteorol.* 35, 987–992.
- Malbéteau, Y., Merlin, O., Molero, B., Rüdiger, C., Bacon, S., 2015. DisPATCH as a tool to evaluate coarse-scale remotely sensed soil moisture using localized in situ measurements: Application to SMOS and AMSR-E data in Southeastern Australia. *Int. J. Appl. Earth Obs. Geoinf.* 45, 221–234.
- Masson, V., Le Moigne, P., Martin, E., Faroux, S., Alias, A., Alkama, R., Voldoire, A., 2013. The SURFEXv7.2 land and ocean surface platform for coupled or offline simulation of earth surface variables and fluxes. *Geosci. Model Dev.* 6, 929–960.
- Merlin, O., Escorihuela, M.J., Mayoral, M.A., Hagolle, O., Albitar, A., Kerr, Y., 2013. Self-calibrated evaporation-based disaggregation of SMOS soil moisture: an evaluation study at 3 km and 100 m resolution in Catalonia, Spain. *Remote Sens. Environ.* 130, 25–38.
- Merlin, O., Rüdiger, C., Al Bitar, A., Richaume, P., Walker, J., Kerr, Y., 2012. Disaggregation of SMOS soil moisture in southeastern Australia. *IEEE Trans. Geosci. Remote Sens.* 50, 1556–1571.
- Merlin, O., Walker, J.P., Chehbouni, A., Kerr, Y., 2008. Towards deterministic downscaling of SMOS soil moisture using MODIS derived soil evaporative efficiency. *Remote Sens. Environ.* 112, 3935–3946.
- Mittelbach, H., Seneviratne, S.I., 2012. A new perspective on the spatio-temporal variability of soil moisture: temporal dynamics versus time-invariant contributions. *Hydrol. Earth Syst. Sci.* 16, 2169–2179.
- Molero, B., Merlin, O., Malbéteau, Y., Al Bitar, A., Cabot, F., Stefan, V., Kerr, Y., Bacon, S., Cosh, M.H., Bindlish, R., Jackson, T.J., 2016. SMOS disaggregated soil moisture product at 1 km resolution: processor overview and first validation results. *Remote Sens. Environ.* 180, 361–376.
- Morbidelli, R., Saltalippi, C., Flammìni, A., Cifrodelli, M., Dari, J., Corradini, C., García-Marin, A.P., Moramarco, T., 2019. On the applicability of temporal stability analysis to raingauge network design. *Hydrol. Sci. J.* 64, 1424–1438.
- Naeimi, V., Scipal, K., Bartalis, Z., Hasenauer, S., Wagner, W., 2009. An improved soil moisture retrieval algorithm for ERS and METOP scatterometer observations. *IEEE Trans. Geosci. Remote Sens.* 47, 1999–2013.
- Noilhan, J., Mahfouf, J., 1996. The ISBA land surface parameterisation scheme. *Glob. Planet. Change* 13, 145–159.
- Noilhan, J., Planton, S., 1989. A simple parameterization of land surface processes for meteorological models. *Mon. Weather Rev.* 117, 536–549.
- O'Neill, P.E., Chan, S., Njoku, E.G., Jackson, T., Bindlish, R., 2016. SMAP enhanced L3 radiometer global daily 9 km EASE-grid soil moisture, version 1. L2_SM_P-E. Boulder, CO: NASA National Snow and Ice Data Center Distributed Active Archive Center. <https://doi.org/10.5067/ZRO7EXJ8O3XI>.
- Ozdogan, M., Gutman, G., 2008. A new methodology to map irrigated areas using multi-temporal MODIS and ancillary data: an application example in the continental US. *Remote Sens. Environ.* 112, 3520–3537.
- Ozdogan, M., Yang, Y., Allez, G., Cervantes, C., 2010. Remote sensing of irrigated agriculture: opportunities and challenges. *Remote Sens.* 2, 2274–2304.
- Peng, J., Loew, A., Merlin, O., Verhoest, N.E.C., 2017. A review of spatial downscaling of satellite remotely sensed soil moisture. *Rev. Geophys.* 55, 341–366.
- Peña-Arancibia, J.L., McVicar, T.R., Paydar, Z., Li, L., Guerschman, J.P., Donohue, R.J., Dutta, D., Podger, G.M., van Dijk, A.I.J.M., Chiew, F.H.S., 2014. Dynamic identification of summer cropping irrigated areas in a large basin experiencing extreme climatic variability. *Remote Sens. Environ.* 154, 139–152.
- Poe, G., 1990. Optimum interpolation of imaging microwave radiometer data. *IEEE Trans. Geosci. Remote Sens.* 28 (5), 800–810.
- Pullainen, J.T., Manninen, T., Hallikainen, M.T., 1998. Application of ERS-1 wind scatterometer data to soil moisture monitoring in boreal forest zone. *IEEE Trans. Geosci. Remote Sens.* 34, 758–770.
- Rockström, J., Falkenmark, M., Lannerstad, M., Karlberg, L., 2012. The planetary water drama: dual task of feeding humanity and curbing climate change. *Geophys. Res. Lett.* 39, L15401.
- Romaguera, M., Krol, M., Salama, M., Su, Z., Hoekstra, A., 2014. Application of a remote sensing method for estimating monthly blue water evapotranspiration in irrigated agriculture. *Remote Sens.* 6, 10033–10050.
- Rosegrant, M.W., Meijer, S., Cline, S.A., 2002. International Model for Policy Analysis of Agricultural Commodities and Trade (IMPACT), Model Description, IFPRI: Washington, DC, USA.
- Siebert, S., Henrich, V., Frenken, K., Burke, J., 2013. Global Map of Irrigation Areas version 5. Rheinische Friedrich-Wilhelms-University, Bonn, Germany/Food and Agriculture Organization of the United Nations, Rome, Italy.
- Stogryn, A., 1978. Estimates of brightness temperatures from scanning radiometer data. *IEEE Trans. Antennas Propag.* AP-26, 720–726.
- Teluguntla, P., Thenkabail, P.S., Xiong, J., Gumma, M.K., Congalton, R.G., Oliphant, A., et al., 2017. Spectral matching techniques (SMTs) and automated cropland classification algorithms (ACCAs) for mapping croplands of Australia using MODIS 250-m time-series (2000–2015) data. *Int. J. Digit. Earth* 8947, 1–34.
- Thenkabail, P.S., Parthasaradhi, G., Biggs, T.W., Gumma, M.K., Tural, H., 2007. Spectral matching techniques to determine historical land use/land cover (ULC) and irrigated areas using time-series AVHRR Pathfinder datasets in the Krishna river basin, India. *Photogramm. Eng. Remote Sens.* 73, 1029–1040.
- Vachaud, G., Passerat de Silans, A., Balabanis, P., Vaucelin, M., 1985. Temporal stability of spatial measured soil water probability density function. *Soil Sci. Soc. Am. J.* 49, 822–828.
- Vörösmarty, C.J., Green, P., Salisbury, J., Lammers, R.B., 2000. Global water resources: vulnerability from climate change and population growth. *Science* 289, 284–288.
- Wada, Y., Wisser, D., Bierkens, M.F.P., 2014. Global modeling of withdrawal, allocation and consumptive use of surface water and groundwater resources. *Earth Syst. Dyn.* 5 (1), 15–40.
- Wagner, W., Blöschl, G., Pampanoni, P., Calvet, J.C., Bizzarri, B., Wigneron, J.P., Kerr, Y., 2007. Operational readiness of microwave remote sensing of soil moisture for hydrologic applications. *Nord. Hydrol.* 38, 1–20.
- Wagner, W., Hahn, S., Kidd, R., Melzer, T., Bartalis, Z., Hase-nauer, S., Figa-Saldana, J., de Rosnay, P., Jann, A., Schneider, S., Komma, J., Kubu, G., Brugger, K., Aubrecht, C., Züger, J., Gangkofner, U., Kienberger, S., Brocca, L., Wang, Y., Blöschl, G., Eitzinger, J., Steinnocher, K., 2013. The ASCAT soil moisture product: a review of its specifications, validation results, and emerging applications. *Meteorologische Zeitschrift*, 22, 5–33.
- Wagner, W., Lemoine, G., Rott, H., 1999. A method for estimating soil moisture from ERS scatterometer and soil data. *Remote Sens. Environ.* 70, 191–207.
- Wen, J., Su, Z.B., 2003. A time series based method for estimating relative soil moisture with ERS wind scatterometer data. *Geophys. Res. Lett.* 30, 1397.
- Zaussinger, F., Dourigo, W., Gruber, A., Tarpanelli, A., Filippucci, P., Brocca, L., 2019. Estimating irrigation water use over the contiguous United States by combining satellite and reanalysis soil moisture data. *Hydrol. Earth Syst. Sci.* 23, 897–923.
- Zhou, T., Haddeland, I., Nijssen, B., Lettenmaier, D.P., 2016. Human-induced changes in the global water cycle. *Terrestrial Water Cycle and Climate Change: Natural and Human-Induced Impacts*, Geophysical Monograph, first ed., 221.